Mechanism and Kinetics of Low-Temperature Oxidation of a Biodiesel Surrogate: Methyl Propanoate Radicals with Oxygen Molecule

ARTICLE *in* THE JOURNAL OF PHYSICAL CHEMISTRY A · APRIL 2015

Impact Factor: 2.69 · DOI: 10.1021/jp5128282

4 AUTHORS:

Xuan T. Le
Institute for Computational Science and Tec…
7 PUBLICATIONS **6** CITATIONS
SEE PROFILE

Tam Mai
Institute for Computational Science and Tec…
8 PUBLICATIONS **6** CITATIONS
SEE PROFILE

Artur Ratkiewicz
University of Bialystok
36 PUBLICATIONS **373** CITATIONS
SEE PROFILE

Lam Huynh
Vietnam National University, Ho Chi Minh City
40 PUBLICATIONS **578** CITATIONS
SEE PROFILE

THE JOURNAL OF PHYSICAL CHEMISTRY A

Article

Mechanism and Kinetics of Low-temperature Oxidation of a Biodiesel Surrogate - Methyl Propanoate Radicals with Oxygen Molecule

Xuan T. Le, Tam V.-T. Mai, Artur Ratkiewicz, and Lam K Huynh

J. Phys. Chem. A, **Just Accepted Manuscript** • DOI: 10.1021/jp5128282 • Publication Date (Web): 30 Mar 2015

Mechanism and Kinetics of Low-Temperature Oxidation of a Biodiesel Surrogate - Methyl Propanoate Radicals with Oxygen Molecule

Xuan T. Le,[a] Tam V.T Mai,[a] Artur Ratkiewicz[b] and Lam K. Huynh[a,c]*

[a] *Institute for Computational Science and Technology at Ho Chi Minh City;*

[b] *Institute of Chemistry, University of Bialystok, ul Hurtowa 1 15-399 Białystok Poland*

[c] *International University, Vietnam National University - HCMC*

---

*Corresponding authors. Email address: hklam@hcmiu.edu.vn / hklam@icst.org.vn (LKH)
Tel: (84-8) 2211.4046 (Ext. 3233) Fax: (84-8) 3724.4271

Graphical Abstract

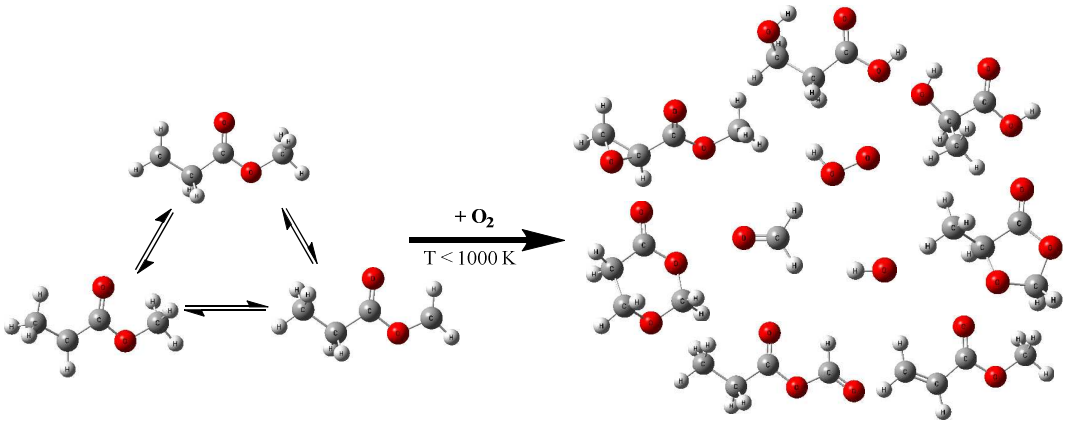

Abstract

This paper presents a computational study on the low-temperature mechanism and kinetics of the reaction between molecular oxygen and alkyl radicals of methyl propanoate (MP), which plays an important role in low-temperature oxidation and/or auto-ignition processes of the title fuel. Their multiple reaction pathways either accelerate the oxidation process via chain branching or inhibit it by forming relatively stable products. The potential energy surfaces of the reactions between three primary MP radicals and molecular oxygen, namely, $C\bullet H_2CH_2COOCH_3 + O_2$, $CH_3C\bullet HCOOCH_3 + O_2$ and $CH_3CH_2COOC\bullet H_2 + O_2$, were constructed using the accurate composite CBS-QB3 method. Thermodynamic properties of all species as well as high-pressure rate constants of all reaction channels were derived with explicit corrections for tunneling and hindered internal rotations. Our calculation results are in good agreement with a limited number of scattered data in the literature. Furthermore, pressure- and temperature-dependent rate constants for all reaction channels on the multiwell-multichannel potential energy surfaces were computed with the Quantum Rice–Ramsperger–Kassel (QRRK) and the modified strong collision (MSC) theories. This procedure resulted in a thermodynamically-consistent detailed kinetic sub-mechanism for low-temperature oxidation governed by the title process. A simplified mechanism, which consists of important reactions, is also suggested for low-temperature combustion at engine-liked conditions.

Keywords: biodiesel surrogate, methyl propanoate, pressure-dependent rate constants, low-temperature oxidation, thermodynamics and detailed kinetic mechanism.

1. Introduction

Biodiesel fuels are often produced from mono-alkyl esters of long-chain fatty acids derived from vegetable oils and animal fats. Typically, they have the structure of a methyl ester group attached to a long hydrocarbon chain of about 16-19 carbon atoms ($C_{16\text{-}19}H_x$-C(=O)O-CH_3). Due to the presence of the heterogeneous oxygen atom as in the ester functional group (–COO–), compared to the traditional hydrocarbon fuels, their physical and chemical properties/behaviors are expected to be different. Specifically, it is a more environmentally-friendly fuel with low emission of pollutants such as carbon monoxide, carbon dioxide, sulfur compounds and particulate matter,[1] while its effects on nitrogen oxides (NO_x) remain uncertain. Such NO_x emissions have been experimentally observed either increasingly[2, 3] or decreasingly[4] with the use of biodiesel as an alternative fuel or a blend component. Therefore, there is a need for further investigation to shed more light on benefits, drawbacks of biodiesel fuels as well as its influence on operational conditions of engines so that we can take full advantage of this type of alternative fuels.

However, due to their large size and chemical/physical complexity, detailed kinetic study on these biodiesel molecules is very challenging both experimentally and computationally. To meet these challenges, simple molecules referred to as surrogates are normally used to emulate the physical and chemical properties of real conventional fuels that are too complicated for detailed investigation. Computationally, an effective approach is to study small surrogate systems with accurate methods and then extrapolate the known chemistry/physics to larger systems (if applicable) in terms of structure-based rate constant relationship (or rate rules).[5-7] Once those rate rules are established, they can be used to construct the detailed kinetic mechanism for larger real systems using available automatic reaction mechanism generating software.[8-14]

Therefore, it is necessary to determine optimal surrogate models which are small enough to be investigated using accurate calculations but also large enough to represent the chemistry/physics of real molecules. Such good surrogate models will allow us to investigate the oxidation of real methyl esters in an internal combustion engine.[15-22] In this context, methyl propanoate (MP) was chosen for such purposes. It is worth noting that MP radicals were found to be a cracking intermediate/product with relatively high concentrations in the pyrolysis of biodiesel such as the rapeseed methyl ester (RME);[23] therefore, understanding of the oxidation mechanism and kinetics of MP will significantly contribute to the development of reliable kinetic models for larger methyl esters and biodiesels.[24]

The focus of this study is to provide *first-principles* based kinetic data for characterizing of MP radicals + O_2 reactions which, like in the analogous alkyl systems, are believed to play an important role in low-temperature oxidation and auto-ignition processes.[16] Based on the well-constructed potential energy surfaces (PESs) explored at the high-level composite method CBS-QB3, the detailed kinetic analysis is carried out to investigate the kinetic behavior of this system in low-temperature combustion conditions. In order to achieve accurate kinetic predictions of complex chemical systems, it is necessary to incorporate pressure dependence into kinetic models. This is done under the framework of the Quantum Rice-Ramsperger-Kassel (QRRK) and the modified strong collision (MSC) theories.[25] The detailed kinetic mechanism for the title reaction, MP radicals + O_2, is then compiled in the CHEMKIN format for a wide range of temperatures and pressures. A simplified mechanism, which consists of only the most important reactions, is also suggested for low-temperature combustion at engine-liked conditions.

2. Computational Details

2.1. Electronic Structure Calculations

The electronic structure calculations were carried out using the GAUSSIAN 09[26] program. Among different correlated methods considered available, the composite method CBS-QB3,[27] which was previously validated for its ability to accurate predict PES data for the analogous alkyl + O_2 systems,[28, 29] is expected to be the method of choice in terms of accuracy and computation time. This method was successfully used to study thermodynamics and kinetics of similar and larger oxygenated systems. For example, it was applied to investigate methyl-ester peroxy radical decomposition in the low-temperature oxidation of methyl butanoate.[30] CBS-QB3 data were also used to derive group additive values for different oxygenated compounds[31-33]; bond dissociation energies and enthalpies of formation of methyl/ethyl butanoate;[34] oxidation of methyl and ethyl butanoates;[35] and abstraction reaction between MP and hydroxyl radical[36] in which CBS-QB3 is the method of choice to refine the energy for the BH&HLYP and MP2 geometries. A good agreement on calculated reaction barriers and energies for several important reactions was also observed with those by other methods, namely G3, G3B3 and G4 (cf. see Supplementary Table S2).

All reported results for stable molecules as well as transition states (first-order saddle points on the PESs) were obtained with the lowest-energy conformer of a given species. Normal-mode analysis was performed to verify the nature of each of these stationary points. For complicated reaction pathways, in order to confirm the correct transition state, the minimum energy paths (MEP) from the transition state to both the reactants to products were calculated using the intrinsic reaction path (IRC) following method.[37, 38]

2.2. Thermodynamic Property Calculations

The atomization method was employed to calculate the heats of formation of all species and standard statistical mechanics methods were used to calculate thermodynamic properties such as entropies and heat capacities. Because only relative energies are required in this work, no attempts were made to improve the heats of formation using, for example, bond additivity corrections. All harmonic frequencies were scaled by a factor of 0.99 as recommended by Petersson and coworkers[27] prior to their use. It has been shown that the use of the scale factor of 0.99 gives reliable results, for both enthalpy and entropy, for similar methyl acetate (MA) radical + O_2 system.[39] Some low-frequency vibrational modes, which are better treated as internal rotations around single bonds, were replaced in the thermodynamic calculations by an explicit evaluation of the hindered rotations in the most accurate manner as described in our previous work.[39]

2.3. Rate Constant Calculations

The high-pressure rate constants for elementary reactions were calculated using canonical transition state theory (TST) with tunneling corrections based on asymmetric Eckart potentials.[40] Pressure- and temperature- dependent rates for the multiwell-multichannel PES were calculated based on a steady-state analysis, in which the energy-dependent unimolecular rate coefficients *k(E)* were computed using the QRRK theory.[25] The vibrational frequencies needed to calculate the density of states were extracted from the analysis of the heat capacities, obtained from the CBS-QB3 data. Collisional stabilization rate constants were calculated using the modified strong collision assumption (MSC).[25] The high-pressure kinetic data for the barrierless recombination of MP radicals with O_2 were derived from similar data for alkyl + O_2 systems.[28, 29] In the same vein, the Lennard-Jones collision diameters (σ_{LJ}) of 6.205 Å and well depths

(ε_{LJ}) of 721.3 K were estimated from similar systems.[41] To calculate stabilization rate constants the average energy transferred per collision $\langle E_{all} \rangle$ = 440 cal/mol[28] for the bath gas collider of N_2 ($\sigma_{LJ} = 3.80$ Å, $\varepsilon_{LJ} = 71.4$ K)[41] was assumed. The calculations were also performed with He as the bath gas ($\langle E_{all} \rangle$ = 250 cal/mol;[28] $\sigma_{LJ} = 2.55$ Å and $\varepsilon_{LJ} = 10.2$ K[41]). The simulation results (provided in the accompanied Supplementary material) were generally found to be rather insensitive to the nature of the collider, at least for the conditions considered in this study.

3. Results and Discussion

In the section below, we first report the CBS-QB3 potential energy surfaces (PESs) of the reactions between molecular oxygen with the three primary MP radicals, namely •$CH_2CH_2C(=O)OCH_3$ (**R1**), CH_3C•$HC(=O)OCH_3$ (**R2**) and $CH_3CH_2C(=O)OC$•H_2 (**R3**). The appropriate pathways are then discussed to highlight important channels energetically. Furthermore, thermodynamic properties of all species as well as high-pressure rate constants of all reaction channels with explicit corrections for tunneling and hindered internal rotations are derived and compared with literature data. The pressure-dependent analysis is carried out within the QRRK/RRKM framework. This analysis results in a thermodynamically consistent detailed kinetic mechanism for low-temperature oxidation of the title reactions. In addition, important reactions at the conditions of interest (e.g., engine-liked conditions) are identified, which opens the possibility to derive rate rules to larger similar systems.

The three primary MP radicals can isomerize to each other through the hydrogen migration reactions via different ring transition states (cf. Figure 1) whose barriers depend on the reaction type. As discussed in the literature[42], the barrier heights

increase as the size of the ring in the transition states decrease. The same trend, confirmed further in this study, is also true for the reverse reactions.

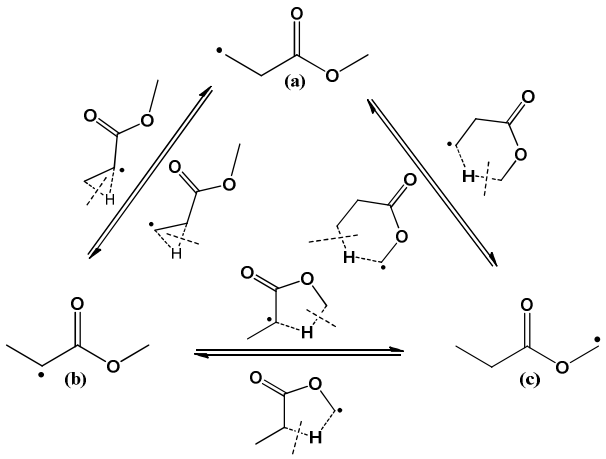

Figure 1. Three MP radicals formed by breaking C – H bond: (a) 3-methoxy-3-oxopropyl, $\bullet CH_2CH_2C(=O)OCH_3$ (**R1**); (b) 1-methoxy-1-oxopropan-2-yl, $CH_3C\bullet HC(=O)OCH_3$ (**R2**); (c) propanoyloxy methyl, $CH_3CH_2C(=O)OC\bullet H_2$ (**R3**). The symbol "•" is denoted the radical position. These radicals can isomerize through hydrogen migration reactions whose transition states are given below and above the reversible arrows.

3.1. Potential Energy Surfaces

Formation/stabilization of initially-formed adducts ROO•. This reaction is the main channel of the complex process, governing the low-temperature fuel behavior. The strength of the formed C-OO bond in the alkyl peroxy radicals (or the ROO• well depth) determines the importance of the collisional stabilization channel and the temperature and pressure at which this reaction plays a role. Re-dissociation of ROO• is believed to be the main cause of the negative-temperature coefficient (NTC) effect.[43] Due to the presence of the ester group –C(=O)O–, it is expected that the behavior of biodiesel surrogates, including the methyl propanoate studied here, is different from that of the analogous alkyl systems.

The C-OO bond energy at 298 K increases in the order of $CH_3HC(OO\bullet)C(=O)OCH_3$, $CH_3CH_2C(=O)OCH_2OO\bullet$ and $\bullet OOCH_2CH_3C(=O)OCH_3$ (25.5, 34.3 and 34.9 kcal/mol, respectively). It is noted that for the methyl acetate radicals, the values are 25.5 and 33.9 kcal/mol for $\bullet OOCH_2C(=O)OCH_3$ and $CH_3C(=O)OCH_2OO\bullet$, respectively,[39] and the numbers are 35.6 and 37.4 kcal/mol for general primary and secondary carbon sites, respectively.[5, 44] The difference in the C—OO bond energy between the two systems (i.e., methyl ester alkyl and alkyl, suggest that the ester group has significant effect on the nearest radical site connected to the ester carbon (e.g., at $\bullet CH_2C(=O)OCH_3$ and $CH_3C\bullet HC(=O)OCH_3$). This observation can be explained in terms of the hyper-conjugation effect as discussed for methyl acetate radicals + O_2 system[39] and for similar alkyl + O_2 systems.[5, 44, 45]

Figures 2-4 present the PESs at 0 K for the three systems established at the CBS-QB3 level. Because of the large number of propagation reactions involved, unimportant pathways (i.e., having the barrier higher than 12 kcal/mol above the entrance channel) are not included. Optimized geometries of all species with important geometrical parameters at the CBS-QB3 level are provided in Supplementary Table S7. Detailed molecular information of the involved species can be found in Supplementary Table S7. To facilitate the discussion, the CBS-QB3 energies at 0 K are used universally and are cited relatively to the reactant energy; otherwise, it is explicitly stated.

$\bullet CH_2CH_2C(=O)OCH_3 + O_2$ system.

Figure 2 shows the calculated CBS-QB3 potential energy diagram for the $\bullet CH_2CH_2C(=O)OCH_3$ + O_2 system at 0 K. The initially-formed adduct $\bullet OOCH_2CH_2C(=O)OCH_3$ (**I1**) can react through several reaction pathways, namely, re-dissociation back to the reactant, isomerization to different intermediates, or

dissociation to different bimolecular products. The lowest energy channel is to form methyl acrylate through the concerted HO_2 elimination reaction (**P3** channel), which proceeds via a planar five-membered ring transition state (**TS1)** with the barrier height of 27.1 kcal/mol (6.9 kcal/mol below the entrance channel). Due to the effect of the ester group, the barrier of this channel is about 3 kcal/mol lower than those at the same primary carbon of the alkyl systems (e.g., 30.9 and 29.7 kcal/mol for *n*-propyl radical by Huynh et al.[29] and DeSain et al.,[46] respectively). This low-energy channel is expected to play a role at the low temperature and/or high pressure.

Alternatively, **I1** can form methyl 3-oxopropanoate ($O{=}CHCH_2C(=O)OCH_3$) and OH (**P1** products) through the 1-3s H-transfer transition state (**TS2)** with barrier energy of 41.7 kcal/mol (7.7 kcal/mol above the entrance channel). The H-transfer notation refers to the position of the heavy atoms involved in the transition state and the type of radical produced (e.g., primary, secondary or tertiary) which was adopted from the work of Goldsmith and coworkers.[47] The isomerization product ($HOOC\bullet HCH_2C(=O)OCH_3$) is unstable; thus it can easily dissociate to $O{=}CHCH_2C(=O)OCH_3$ and OH. The adduct **I1** can also isomerize to form two isomers, namely, $HOOCH_2C\bullet HC(=O)OCH_3$ (**I2**) and $HOOCH_2CH_2C(=O)OC\bullet H_2$ (**I3**). **I2** can dissociate to form bimolecular products such as methyl acrylate + HO_2 via **TS8** (β-scission reaction) and methyl oxirane-2-carboxylate ($cy[H_2COCH]CC(=O)OCH_3$) + OH via **TS6** (cyclization reaction) with the barrier, $\Delta V^{\neq}$, of 18.3 kcal/mol and 17.6 kcal/mol, respectively. Even though **I2** is more stable; **I3** can be formed easier from **I1** since it proceeds via 1-7p H-migration with eight-membered ring transition state (**TS4** with $\Delta V^{\neq}$ = 27.8 kcal/mol) compared to 1-4s H-migration with five-member ring transition state (**TS3** with $\Delta V^{\neq}$ = 33.2 kcal/mol). **I3** can also be formed from **I2** through **TS5** with a much higher barrier than the formation of **I5** via **TS7**, with barrier of 23.9

kcal/mol. This intermediate can isomerize to form •$OCH_2CH_2C(=O)OCH_2OH$ (**I6**) lying at 75.9 kcal/mol below the entrance channel via 1-6 OH transfer reaction (**TS9**) with barrier height of 19.2 kcal/mol. Alternatively, this intermediate can form $HOOCH_2CH_2C$•=O (**I4**) + formaldehyde (at 1.8 kcal/mol) via β-scission reaction **TS10** ($\Delta V^{\neq}$ = 31.0 kcal/mol) and the 1,3-dioxan-4-one (cy[$CH_2CH_2C(=O)OCH_2O$]) + OH (-56.1 kcal/mol) though the cyclization reaction via **TS11** ($\Delta V^{\neq}$ = 21.1 kcal/mol).

The potential energy diagram for the •$CH_2CH_2C(=O)OCH_3$ + O_2 system is very complicated with 03 wells/intermediates and many interconnecting channels. The formation of the initially-formed adduct is the first and the most important event for the evolution of the system. Among all possible reactions of the adduct **I1**, the dissociation back to the reactants and the concerted HO_2 elimination dominate the isomerization channels; therefore, the subsequent reactions of isomerization products seem to be of little importance. The kinetic analysis presented further in this study confirms this expectation.

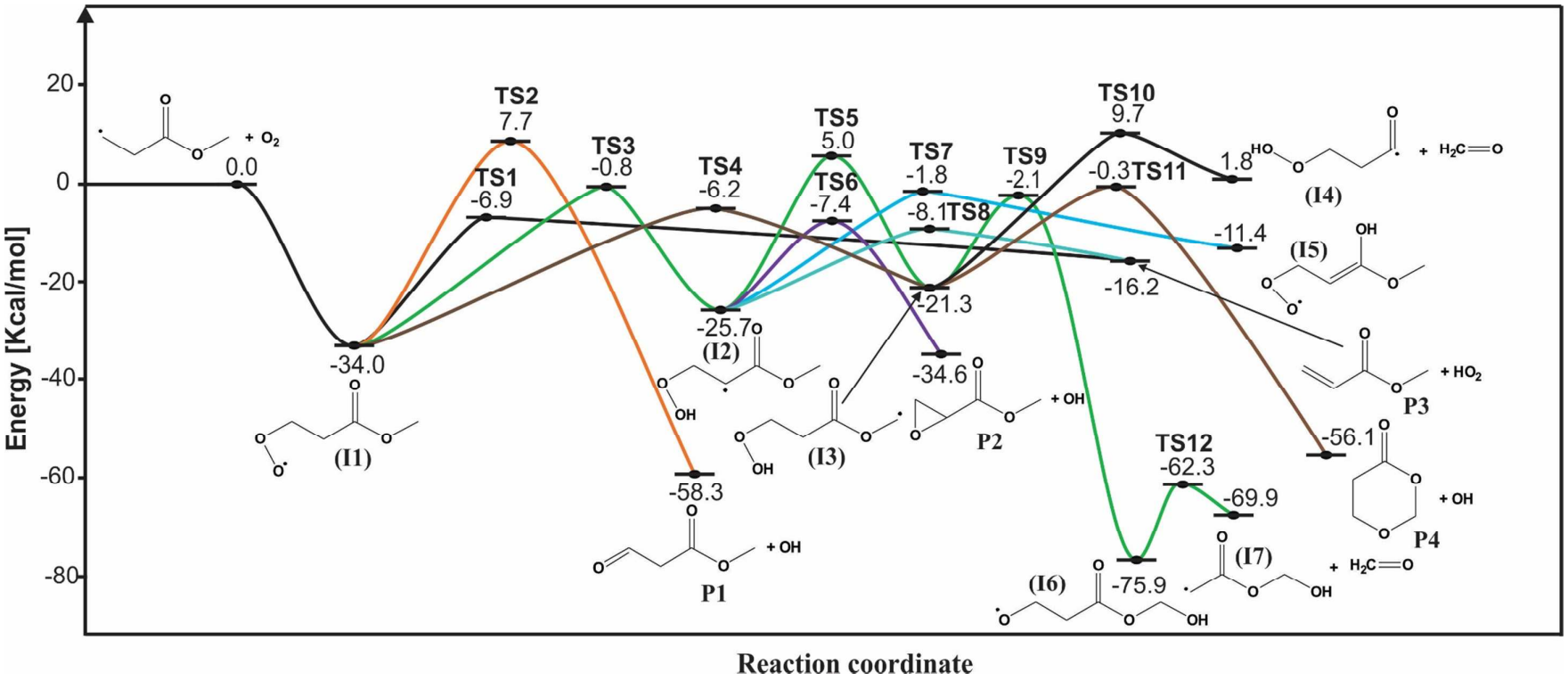

Figure 2. Potential energy diagram for the •$CH_2CH_2C(=O)OCH_3$ + O_2 system at 0 K, calculated at the composite CBS-QB3 level. Numbers are the energies relative to that of the reactants and channels (having energy higher than 12 kcal/mol above the entrance channel) are not included. Hydrogen is not explicitly given in the molecular formula for simplicity, unless it involves in the considered reactions and/or it is for clarity.

$CH_3C\bullet HC(=O)OCH_3 + O_2$ system

A simplified scheme of the reaction network starting from $CH_3C\bullet HC(=O)OCH_3$ is presented in Figure 3. Similar to the first system, the formation of the initial-adduct radical, $CH_3HC(OO\bullet)C(=O)OCH_3$ (**I8**), is a barrierless process with a smaller well-depth (24.9 vs. 34.0 kcal/mol for **I8** and **I1**, respectively); thus it is expected that the effect of the ester group is more profound at this system. The adduct **I8** can form methyl acrylate through concerted HO_2 elimination reaction via **TS15** with the barrier of 27.2 kcal/mol (2.3 kcal/mol above the entrance channel) which is smaller than that of i-propyl system ($\Delta V^{\neq}$ = 31.2 kcal/mol[29]), thus it is expected to be the dominant pathway to form methyl acrylate and HO_2. In addition to the concerted channel, adduct **I8** can proceed through two isomerization channels: H atom transfer from a methyl group to the peroxy radical site via a seven-member ring (**TS13**) to form $CH_3HC(OOH)C(=O)OC\bullet H_2$ (**I9**) and via a five-member ring (**TS14**) to $\bullet CH_2HC(OOH)C(=O)OCH_3$ (**I10**) with the barrier of 30.5 and 36.2 kcal/mol, respectively. The former isomer can dissociate to two bimolecualr products, where the formation of the cyclic CH_3cy[$HCC(=O)OCH_2O$] (**P6**) via **TS17** has the barrier of 4.5 kcal/mol smaller than that of $CH_3C(=O)C(=O)OCH_3$ (**P5**) via **TS16** (through H atom transfer from a secondary site to methyl group). The latter isomer can contribute to the formation of methyl acrylate through β-scission reaction (**TS19**) with the barrier of 0.5 kcal/mol lower than that of the channel to methyl oxirane-2-carboxylate (cy[H_2COCH]$C(=O)OCH_3$) through cyclization reaction (**TS18**).

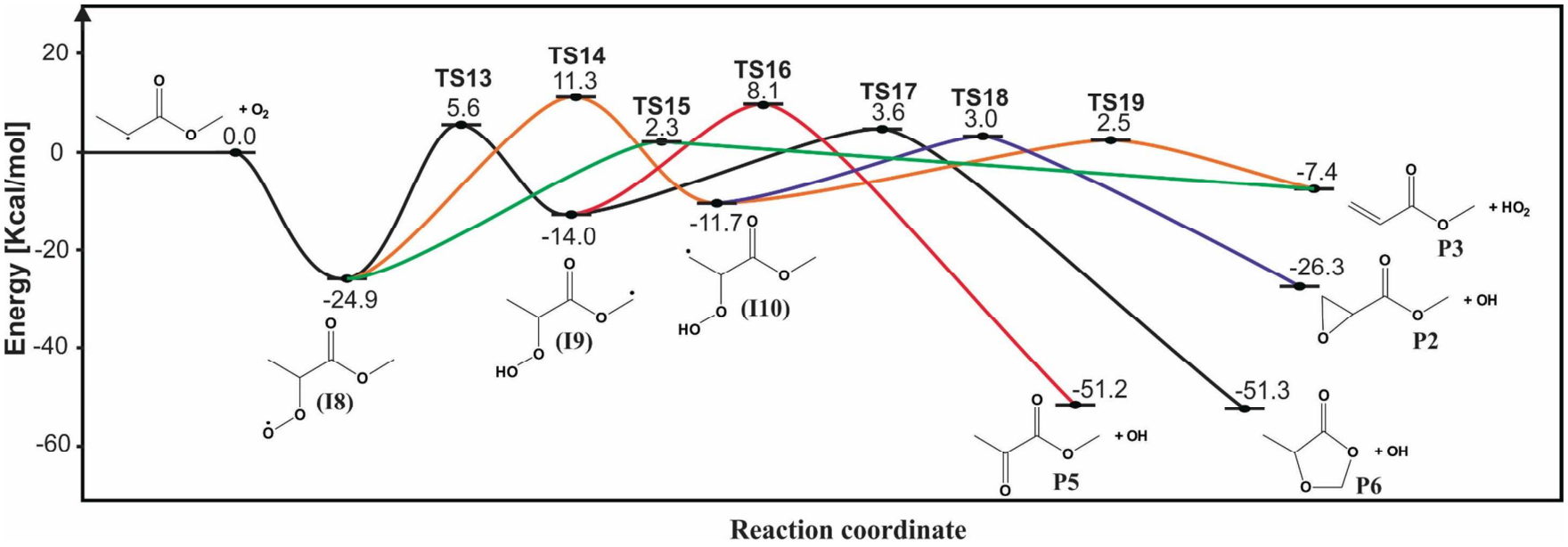

Figure 3. Potential energy diagram for the $CH_3C\bullet HC(=O)OCH_3 + O_2$ system at 0 K, calculated at the composite CBS-QB3 level. Numbers are the energies relative to that of the reactants and channels (having energy higher than 12 kcal/mol above the entrance channel) are not included. Hydrogen is not explicitly given in the molecular formula for simplicity, unless it involves in the considered reactions or it is for clarity.

$CH_3CH_2C(=O)OC\bullet H_2 + O_2$ system

This reaction network is expected to be the most complicated among the three MP radical systems. Figure 4 provides the potential energy surface diagram of this system where only the channels lower than 12 kcal/mol above the entrance are described for the sake of simplicity. The adduct $CH_3CH_2C(=O)OCH_2OO\bullet$ (**I11**) is initially formed via a barrierless reaction with a well depth of 33.5 kcal/mol and 34.3 kcal/mol at 0 and 298 K, respectively. These values agree well with previous calculations for the same radical site of methyl acetate + O_2 by Mai et al.[39] (33.4 and 33.9 kcal/mol at 0 and 298 K respectively) and of methyl butanoate radicals + O_2 by Tao et al.[30] (~34 kcal/mol at 0 K), thus demonstrating that the carbon chain length has a little impact on this radical site. Furthermore, the results for the oxygenated species agree well with similar calculations for the primary carbon site of the *n*-propyl + O_2 system, (34.8 and 35.5 kcal/mol at 0 and 298 K, respectively). This oxygen centered radical experiences the internal H abstraction from any of the three possible carbon sites, one of which is the formation of the stable product (**P8**) from the unstable $CH_3CH_2C(=O)O\ C\bullet(OOH)H$ via a four-member ring (**TS24).** Two other channels lead to reactive intermediates: $\bullet CH_2CH_2C(=O)OCH_2OOH$ (**I13**) via an eight-membered ring transition state **TS21**, and $CH_3C\bullet HC(=O)OCH_2OOH$ (**I12**) via seven-membered ring **TS20,** about 1 kcal/mol higher than **TS21**. The difference between those barriers can be explained mainly through the different strain energies of various TS-ring sizes. The barrier height of the **I11→TS20→I12** channel is equal to 26.7 kcal/mol, which is lower than those of MA+O_2[39] and MB+O_2[30] about 3.8 and 1.8 kcal/mol, respectively. The barrier deviation between the MP and MA can be demonstrated by the difference of the secondary (for MP) and primary (for MA) C-H sites. It is interesting to note that there is no significant difference between barriers for MP and MB (26.7 and 26.5 kcal/mol,

respectively). Intermediate **I12** can dissociate to form several bi-molecular products, among which is the formation of the cyclic CH_3cy[CHC(=O)OCH_2O] and aldehyde (CH_3CH_2C(=O)OCHO) compounds with the barriers comparable to the entrance channel (5.7 and 2.5 kcal/mol below the entrance channel, respectively). The 1-5 hydroxide migration reaction from **I12** to C H_3C(OH)HC(=O)OCH_2O• (**I14)** proceeds with a barrier higher than those of the other processes involving **I12**; thus this channel is expected not to be competitive in the low temperature regime. **I13** can be formed from **I11** via **TS21** with the barrier of 25.7 kcal/mol, which is in excellent agreement with the analogical reaction in the MB + O_2 system (i.e., the difference is less than 0.5 kcal/mol at 0 and 298 K).[30] Although the formation of **I13** has a barrier lower than those of **I12**, **I13** is less stable than **I12** and lies 21.6 kcal/mol below the reactant. As a result, **I13** can easily proceed through four reaction pathways: (1) 1-5s H-atom transfer to form an unstable CH_3CH_2C(=O)OC•(OOH)H via a seven-member ring transition state **TS25** ($\Delta V^{\neq}$ = 20.5 kcal/mol); (2) 1-6 hydroxide migration to form intermediate $HOCH_2CH_2$C(=O)OCH_2O• (**I16**) via **TS28** ($\Delta V^{\neq}$ = 26.3 kcal/mol); (3) cyclization reaction to cy[H_2CCH_2C(=O)OCH_2O] via **TS29** ($\Delta V^{\neq}$ = 20.5 kcal/mol) and (4) β-scission reaction to intermediate •C(=O)OCH_2OOH (**I15**) via **TS30** ($\Delta V^{\neq}$ = 31.9 kcal/mol). The channels (2) and (4) have the barriers much higher than (1) and (3); therefore, they are energetically less favorable.

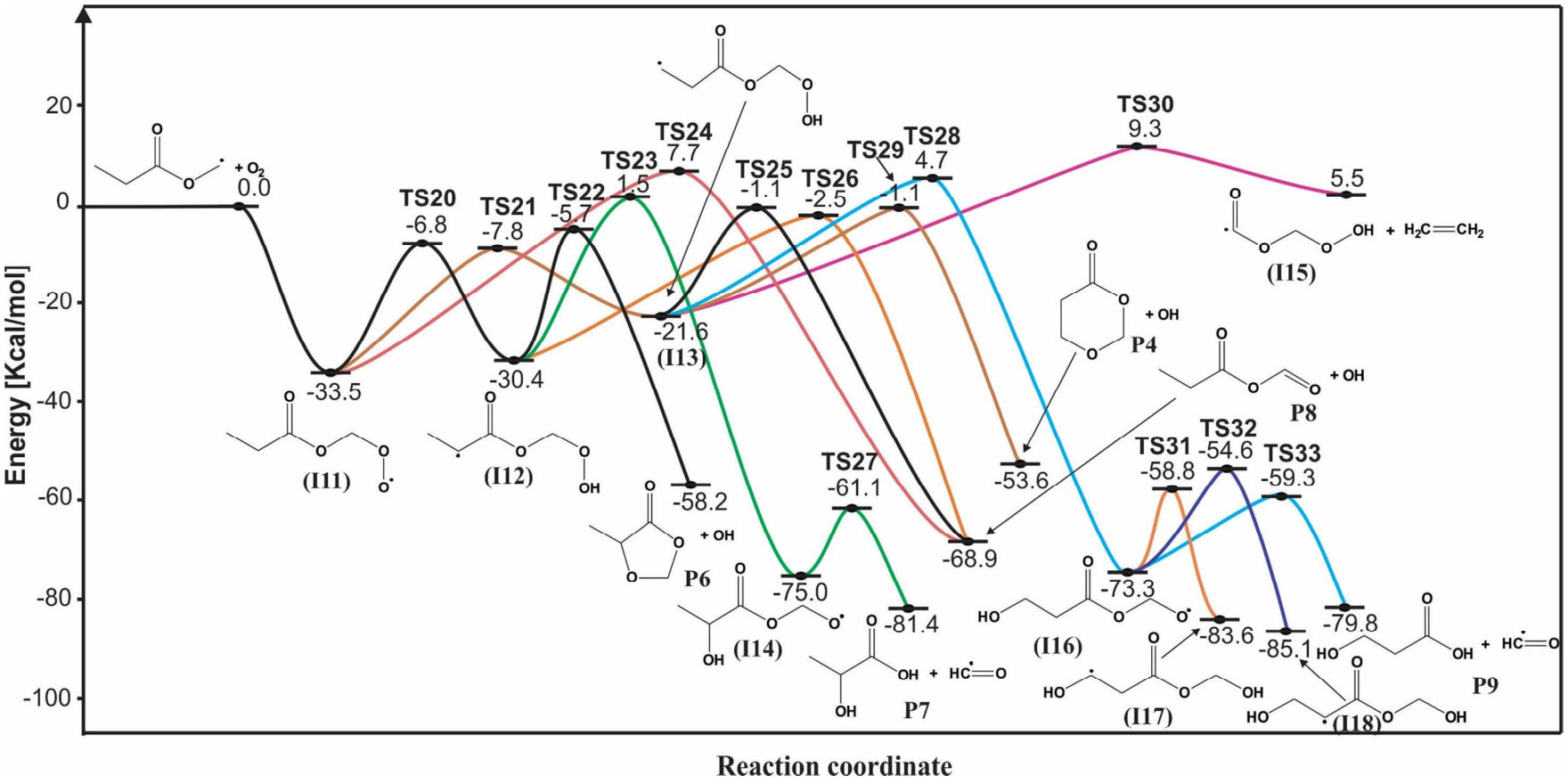

Figure 4. Potential energy diagram for the $CH_3CH_2C(=O)OC\bullet H_2 + O_2$ system at 0 K, calculated at the composite CBS-QB3 level. Numbers are the energies relative to that of the reactants and channels (having energy higher than 12 kcal/mol above the entrance channel) are not included. Hydrogen is not explicitly given in the molecular formula for simplicity, unless it involves in the considered reactions or it is for clarity.

3.2. Thermodynamic Properties

Calculations of thermodynamic properties (heat of formation $\Delta_f H$, entropy S and heat capacity C_p) follow the procedure described in the "Thermodynamic Property Calculations" section above. The thermodynamic properties of species involved in the MP + O_2 systems are limited in the literature. To evaluate the reliability of our results, we provided the literature values along with the calculated numbers for selected species (cf. Table 1) while the calculated data for all species involved can be found in the accompanied supplementary material. The available experimental/calculated data (from Webbook NIST[48] and Active Thermochemical Tables (ATcT)[49, 50]) confirm that our calculated values are within the uncertainty range for $\Delta_f H$, S and $C_{p.}$ The mean average deviation (MAD) between our numbers and ATcT approach are 1.6 kcal/mol for $\Delta_f H^{298\ K}$, 1.5 cal/mol-K for $S^{298\ K}$ and 0.8 cal/mol-K for $C_p^{298\ K}$, while those for NIST data are 1.4 kcal/mol and 2.83 cal/mol-K for $\Delta_f H^{298\ K}$ and $S^{298\ K}$, respectively. That the average differences in $\Delta_f H$ is within chemical accuracy range (1-2 kcal/mol) give us more confidence in our numbers, which are then used for the next calculations.

Table 1. Comparison of Calculated Thermodynamic Properties of Selected Stable Species Involved in the System with Experimental/Calculated Data (ATcT=Active Thermochemical Tables[49, 50][a], NIST[48] = Webbook NIST). Units: kcal/mol for $\triangle_f H^{298}$ and cal/mol-K for S and C_p.

Species	Method	$\Delta_f H^{298}$ [c]	S^{298}	C_p^{300}	C_p^{400}	C_p^{500}	C_p^{600}	C_p^{800}	C_p^{1000}	C_p^{1500}
		kcal/mol	cal/mol-K							
O=CCC(=O)OC	This work[b]	-122.3	91.1	27.6	33.0	38.0	42.2	48.9	53.7	60.9
	NIST	-125.1	97.6	–	–	–	–	–	–	–
cy[CCC(=O)OCO]	This work	-121.4	78.0	23.9	30.9	37.1	42.2	50.0	55.4	63.3
	NIST	–	–	–	–	–	–	–	–	–
CC(=O)C(=O)OC	This work	-123.5	90.1	28.5	33.7	38.3	42.4	48.8	53.5	60.7
	NIST	-121.9	97.9	–	–	–	–	–	–	–
C*cy*[CC(=O)OCO]	This work	-125.7	81.2	25.6	31.8	37.7	42.5	49.9	55.0	62.6
	NIST	–	–	–	–	–	–	–	–	–
HOCCC(=O)OH	This work	-147.7	81.9	25.5	32.1	37.6	42.0	48.1	52.0	57.5
	NIST	-144.4	87.8	25.3	30.7	34.9	38.5	44.3	48.3	–
CCC(=O)OC=O	This work	-135.2	88.8	29.1	34.9	40.2	44.7	51.3	55.9	62.1
	NIST	-129.1	96.1	–	–	–	–	–	–	–
cy[COC]C(=O)OC	This work	-99.1	87.3	26.0	32.4	38.1	42.8	49.7	54.6	61.9
	NIST	-99.9	90.8	–	–	–	–	–	–	–
C=CC(=O)OC	This work	-73.9	81.1	24.3	29.6	34.5	38.7	45.2	49.7	56.5
	ATcT	-17.7[d]	86.0	24.3	29.4	34.2	38.3	44.5	49.0	55.4
	NIST	-74.0	87.4	–	–	–	–	–	–	–
CC(OH)C(=O)OH	This work	-149.1	82.9	26.4	32.6	37.7	41.7	47.3	51.0	56.5
	ATcT	-145.8	84.6	24.3	30.1	35.0	39.0	44.8	48.9	55.0
	NIST	-148.4	87.0	25.1	30.6	35.4	39.1	45.0	49.0	–
CCC(=O)OC	This work	-104.8	87.0	26.2	31.8	37.2	42.0	49.7	55.5	64.3
	ATcT	-104.5	89.8	25.9	31.5	37.0	41.9	49.6	55.4	63.6
	NIST	-103.8	89.3	–	–	–	–	–	–	–
C_2H_4	This work	13.2	52.3	10.2	12.5	14.8	16.7	19.8	22.2	26.1

Species	Method	$\Delta_f H^{298}$ [c]	S^{298}	C_p^{300}	C_p^{400}	C_p^{500}	C_p^{600}	C_p^{800}	C_p^{1000}	C_p^{1500}
		kcal/mol	cal/mol-K							
	ATcT	12.6	52.4	10.3	12.6	14.9	17.0	20.1	22.5	26.2
	NIST	12.5	52.4	10.3	12.7	14.9	16.9	20.1	22.4	26.3
HCHO	This work	-27.3	52.2	8.4	9.3	10.4	11.4	13.2	14.7	16.9
	ATcT	-26.1	52.3	8.5	9.4	10.4	11.5	13.4	14.8	16.9
	NIST	-27.7	52.3	8.5	9.4	10.4	11.5	13.4	14.8	17.0

[a] values collected from Burcat's online database, http://garfield.chem.elte.hu/Burcat/burcat.html (access date: Dec. 2013); [b] Data were calculated at CBS-QB3 level of theory; [c] $\Delta_f H^{298}$ was calculated by atomization method. [d] probably there is a mistake for this species on Burcat's online database.

3.3. Rate Constant Calculations

Pressure dependence analysis under the QRRK framework requires specification of the high-pressure rate coefficients for each reaction pathway. With the exception of the addition of O_2 to MP radicals, whose rate constants were adopted from the analogous propyl + O_2 system,[29] high-pressure rate coefficients for all important reaction pathways were calculated using unadjusted CBS-QB3 results, following the procedure described earlier. Calculated high-pressure rate constants for all individual channels of the MP systems over the temperature range of 300-1500 K are given in Table 2. The rate constants for the reverse reactions, calculated from the corresponding equilibrium constants and the forward rate constants, are also provided in this table. The literature data for those reactions are sparse and mainly given at much narrower temperature range. Herbinet et al.[16] reported rate constants for four types of reactions (Rxn. 4 and 16 in Table 2) whose kinetic data were extrapolated from larger methyl esters (i.e., methyl decanoate). The ratios of our values to Herbinet's data for the two reactions at 1000 K are 1.3 and 2.1, respectively. The deviation is probably due to the influence of the –C(=O)O– group on the C-H bond cleavage. For example, Rxn. 4 in this work (*1-4s* isomerization via a five-membered ring TS) is close to the secondary carbon site bonded to the ester carbon, while the reactions in Herbinet's work are generally taken for 5-membered rings consisting of all secondary carbon sites. Similarly, for Rxn. 16 (*1-4p* isomerization via a five-membered ring TS) the H abstraction is at the site closer to the –C(=O)O– group than in the reaction considered in Herbinet's work. In general, the differences between ours and literature data are small, so we believe that our rate constants, which are systematically derived from the accurate CBS-QB3 level under the solid statistical mechanic framework, could be confidently used for analyzing the effect of pressure as well as extrapolating to larger methyl esters.

Table 2. High-Pressure Rate Constants for Reactions of MP Radicals with O_2 and Comparison with Available Literature Data. Rate Constants Are Given as $k(T) = A \times T^n \times \exp(-E_a/RT)$, Valid for 300-1500 K.[a] Hydrogen Is not Explicitly Given in the Molecule Formula for Simplicity unless it Involves in the Considered Reactions.

No.	Reaction	This work, $k(T) = A \times T^n \times \exp(-E_a/RT)$			Literature for k(T) at 1000 K
		A[b]	n	E (kcal/mol)	
1	•CCC(=O)OC + O_2 → C(OO•)CC(=O)OC	1.48E+12	0.00	-0.61	–
	(reverse reaction)	3.79E+14	0.00	32.96	–
2	C(OO•)CC(=O)OC → C=CC(=O)OC + HO_2	8.93E+05	1.92	25.05	–
	(reverse reaction)	2.60E-01	3.29	6.01	–
3	C(OO•)CC(=O)OC → C(=O)CC(=O)OC + OH	1.52E+04	2.68	37.30	–
	(reverse reaction)	5.79E-02	3.83	60.33	–
4	C(OO•)CC(=O)OC → C(OOH)C•C(=O)OC	7.52E+03	2.54	28.56	1.29E+05[c] (1.71E+05)
	(reverse reaction)	1.43E+11	0.60	22.28	–
5	C(OO•)CC(=O)OC → C(OOH)CC(=O)OC•	4.87E+02	2.35	23.73	–
	(reverse reaction)	4.04E+14	-1.42	13.01	–
6	C(OOH)C•C(=O)OC → C(OOH)CC(=O)OC•	1.52E+08	1.38	28.01	–
	(reverse reaction)	6.61E+12	-0.45	23.58	–
7	C(OOH)C•C(=O)OC → cy[COC]C(=O)OC + OH	6.52E+14	-0.17	19.12	–
	(reverse reaction)	8.03E+03	2.64	25.66	–
8	C(OOH)C•C(=O)OC → C(OO•)C=C(OH)OC	4.98E+11	0.23	22.98	–
	(reverse reaction)	1.29E+11	0.63	8.52	–
9	C(OOH)C•C(=O)OC → C=CC(=O)OC+ HO_2	2.29E+10	1.04	17.66	–
	(reverse reaction)	3.49E-04	4.35	4.89	–
10	C(OOH)CC(=O)OC• → O•CCC(=O)OCOH	3.39E+15	-1.45	18.82	–
	(reverse reaction)	7.71E+11	-0.10	73.52	–
11	C(OOH)CC(=O)OC• → C(OOH)CC•=O + C=O	1.06E+15	-0.57	31.37	–
	(reverse reaction)	7.84E-05	4.18	4.18	–
12	C(OOH)CC(=O)OC• → cy[CCC(=O)OCO] + OH	9.88E+16	-1.72	21.09	–

No.	Reaction	This work, $k(T) = A \times T^n \times \exp(-E_a/RT)$			Literature for k(T) at 1000 K
		A[b]	n	E (kcal/mol)	
	(reverse reaction)	2.69E+03	2.99	54.54	–
13	•OCCC(=O)OCOH → •CC(=O)OCOH + C=O	7.75E+11	0.57	13.94	–
	(reverse reaction)	3.95E+03	2.33	6.56	–
14	CC•C(=O)OC + O_2 → CC(OO•)C(=O)OC	1.48E+12	0.00	-0.61	–
	(reverse reaction)	7.40E+13	0.00	23.59	–
15	CC(OO•)C(=O)OC → CC(OOH)C(=O)OC•	1.39E+03	2.52	26.59	–
	(reverse reaction)	4.67E+09	0.44	16.62	–
16	CC(OO•)C(=O)OC → •CC(OOH)C(=O)OC	1.14E+06	1.96	32.18	3.56E+04[c] (7.56E+04)
	(reverse reaction)	3.21E+09	0.83	19.59	–
17	CC(OO•)C(=O)OC → C=CC(=O)OC + HO_2	5.89E+05	1.94	25.39	–
	(reverse reaction)	9.88E-02	3.42	7.39	–
18	CC(OOH)C(=O)OC• → CC(=O)C(=O)OC + OH	2.53E+07	1.52	19.41	–
	(reverse reaction)	8.08E+04	2.71	31.89	–
19	CC(OOH)C(=O)OC• → Ccy[CC(=O)OCO] + OH	1.61E+12	0.07	17.27	–
	(reverse reaction)	1.53E+03	3.10	54.67	–
20	•CC(OOH)C(=O)OC → cy[COC]C(=O)OC + OH	3.51E+09	1.00	14.21	–
	(reverse reaction)	1.90E+02	3.05	27.61	–
21	•CC(OOH)C(=O)OC → C=CC(=O)OC + HO_2	8.40E+06	1.87	13.23	–
	(reverse reaction)	5.62E-04	4.42	7.33	–
22	CCC(=O)OC• + O_2 → CCC(=O)OCOO•	1.48E+12	0.00	-0.61	–
	(reverse reaction)	1.58E+15	0.00	32.79	–
23	CCC(=O)OCOO• → CC•C(=O)OCOOH	1.15E+04	2.24	22.19	–
	(reverse reaction)	1.48E+12	0.23	21.34	–
24	CCC(=O)OCOO• → •CCC(=O)OCOOH	5.53E+02	2.18	21.33	–
	(reverse reaction)	3.64E+09	0.34	11.07	–
25	CC•C(=O)OCOOH → Ccy[CC(=O)OCO] + OH	2.31E+15	-0.63	25.03	–
	(reverse reaction)	7.88E+04	2.50	51.23	–

No.	Reaction	This work, $k(T) = A \times T^n \times \exp(-E_a/RT)$			Literature for k(T) at 1000 K
		A[b]	n	E (kcal/mol)	
26	CC•C(=O)OCOOH → CC(OH)C(=O)OCO•	1.86E+13	-0.21	31.14	–
	(reverse reaction)	5.40E+10	0.35	75.45	–
27	CCC(=O)OCOO• → CCC(=O)OC(=O) + OH	2.72E+02	3.08	36.21	–
	(reverse reaction)	7.54E+00	3.30	71.35	–
28	•CCC(=O)OCOOH → CCC(=O)OC(=O) + OH	4.91E+06	1.75	17.46	–
	(reverse reaction)	2.05E-02	3.80	62.87	–
29	CC•C(=O)OCQ → CCC(=O)OC=O + OH	1.91E+08	1.55	25.20	–
	(reverse reaction)	4.05E-02	3.78	61.19	–
30	CC(OH)C(=O)OCO• → CC(OH)C(=O)OH + •C=O	5.12E+10	0.72	13.81	–
	(reverse reaction)	5.55E+01	2.64	18.48	–
31	•CCC(=O)OCOOH → HOCCC(=O)OCO•	5.16E+10	0.38	25.18	–
	(reverse reaction)	4.16E+13	-0.37	78.40	–
32	•CCC(=O)OCOOH → cy[CCC(=O)OCO] + OH	5.24E+11	0.01	19.74	–
	(reverse reaction)	1.62E+03	3.01	51.19	–
33	•CCC(=O)OCOOH → •C(=O)OCOOH + C=C	4.02E+14	0.59	32.38	–
	(reverse reaction)	7.30E+03	2.94	3.35	–
34	HOCCC(=O)OCO• → HOC•CC(=O)OCOH	3.94E+13	-0.68	14.37	–
	(reverse reaction)	2.26E+11	-0.20	23.30	–
35	HOCCC(=O)OCO• → HOCC•C(=O)OCOH	1.02E+12	-0.05	17.45	–
	(reverse reaction)	8.73E+14	-0.83	29.68	–
36	HOCCC(=O)OCO• → HOCCC(=O)OH + •C=O	2.05E+12	0.27	14.18	–
	(reverse reaction)	3.46E+00	3.13	18.30	–

[a] The maximum error for fitting to $k(T) = A \times T^n \times \exp(-E_a/RT)$ is generally less than 6% but in a very few cases is about 11%. [b] Units of [s^{-1}] for first-order reactions and [$cm^3mol^{-1}s^{-1}$] for second-order reactions. [c] derived from the work of Herbinet *et al.*[16]

Pressure Dependence Analysis

The current active area in low-temperature and autoignition modeling is the pressure dependence of the branching ratios/fractions of key reactions, e.g., alkyl radicals + O_2.[51-55] The pressure and temperature analyses have been carried out intensively for different systems, e.g., $C_2H_5 + O_2$,[28] $C_3H_7 + O_2$,[28] vinyl + O_2,[25] neo-pentyl + O_2,[56] methylphenyl + O_2,[57] tert-isooctane radical + O_2,[58] acetyl + O_2,[59] and methyl acetate radicals + O_2.[39] Such pressure and temperature dependent behaviors, which are controlled by unimolecular and recombination reactions, were intensively reviewed by Carstensen and Dean;[60] thus the readers can refer to this review or the references cited therein for detailed description on the available theories and their applications.

To quantitatively characterize the pressure dependence of particular reaction channels we first calculated the temperature- and pressure-dependent rate constants for the addition of O_2 to three methyl propanoate radicals using QRRK method, then rate constants for other subsequent processes were derived. Table 3 presents the selected reactions of $\bullet CH_2CH_2C(=O)OCH_3 + O_2$ and $\bullet OOCH_2CH_2C(=O)OCH_3$ from the first well (**I1**) of the PES shown in Figure 2. For the sake of simplicity, thermally activated processes from second and third stabilized isomers (namely, **I2** and **I3**) are omitted.

Table 3: Reactions on the Portion of $\bullet CH_2CH_2C(=O)OCH_3 + O_2$ PES.

$\bullet CH_2CH_2C(=O)OCH_3 + O_2$ channels	
$\bullet CH_2CH_2C(=O)OCH_3 + O_2 \rightarrow \bullet OOCH_2CH_2C(=O)OCH_3$ (**I1**)	(stabilization)
$\bullet CH_2CH_2C(=O)OCH_3 + O_2 \rightarrow CH_2=CHC(=O)OCH_3 + HO_2$	(concerted elimination)
$\bullet CH_2CH_2C(=O)OCH_3 + O_2 \rightarrow HOOCH_2HC\bullet C(=O)OCH_3$ (**I2**)	(isomerization)
$\bullet CH_2CH_2C(=O)OCH_3 + O_2 \rightarrow HOOCH_2CH_2C(=O)OC\bullet H_2$ (**I3**)	(isomerization)
$\bullet OOCH_2CH_2C(=O)OCH_3$ "delayed" channels[a]	
$\bullet OOCH_2CH_2C(=O)OCH_3 \rightarrow CH_2CH_2C(=O)OCH_3 + O_2$	(redissociation)
$\bullet OOCH_2CH_2C(=O)OCH_3 \rightarrow CH_2=CHC(=O)OCH_3 + HO_2$	(concerted elimination)
$\bullet OOCH_2CH_2C(=O)OCH_3 \rightarrow HOOCH_2HC\bullet C(=O)OCH_3$ (**I2**)	(isomerization)
$\bullet OOCH_2CH_2C(=O)OCH_3 \rightarrow HOOCH_2CH_2C(=O)OC\bullet H_2$ (**I3**)	(isomerization)

[a] the term "delayed" is adopted from the work of Carstensen[28]

The pressure and temperature effects on this system can be qualitatively characterized as follows. At low temperature, the total energy of the initially-formed adduct is mainly due to the bond formation, with little additional contribution from the internal energy of the reactants. As a result, the energy available for unimolecular reactions is limited, and bimolecular stabilization dominates, especially at moderate/high pressures. As the temperature increases and additional internal energy is available for the reactants, the unimolecular reactions of the energized adduct become increasingly important. For the $\bullet OOCH_2CH_2C(=O)OCH_3 + O_2$ system, at low temperature the chemically-activated $\bullet OOCH_2CH_2C(=O)OCH_3$* is mainly stabilized via bimolecular collision to $\bullet OOCH_2CH_2C(=O)OCH_3$, except for sufficiently low pressures, at which it also forms bimolecular products via unimolecular reactions. The branching ratios for the four

unimolecular pathways (three product channels and re-dissociation to reactants) depend on both enthalpic and entropic effects which are normally difficult to be quantified on a complex multiple pathway/channel systems. As the temperature increases, dissociation back to reactants becomes more important because this pathway has larger A-factor than the various product channels.[28] Note that the reactions to form isomers are considered reversible whereas those leading to bimolecular products are considered irreversible.

The different reaction types lead to different branching ratios as the pressure changes (at constant temperature). The stabilization channel of a single well system scales linearly with pressure at low pressures where bimolecular collisions are rate limiting, whereas at the high-pressure regime they become pressure independent. Conversely, the chemically activated unimolecular reactions of such a single well system do not depend on pressure at low pressure and become inversely dependent on pressure at high pressure. The pressure-dependence becomes more complex for multiwell-multichannel systems, thus it is essential to properly account for pressure effects in the analysis of complex reactions.

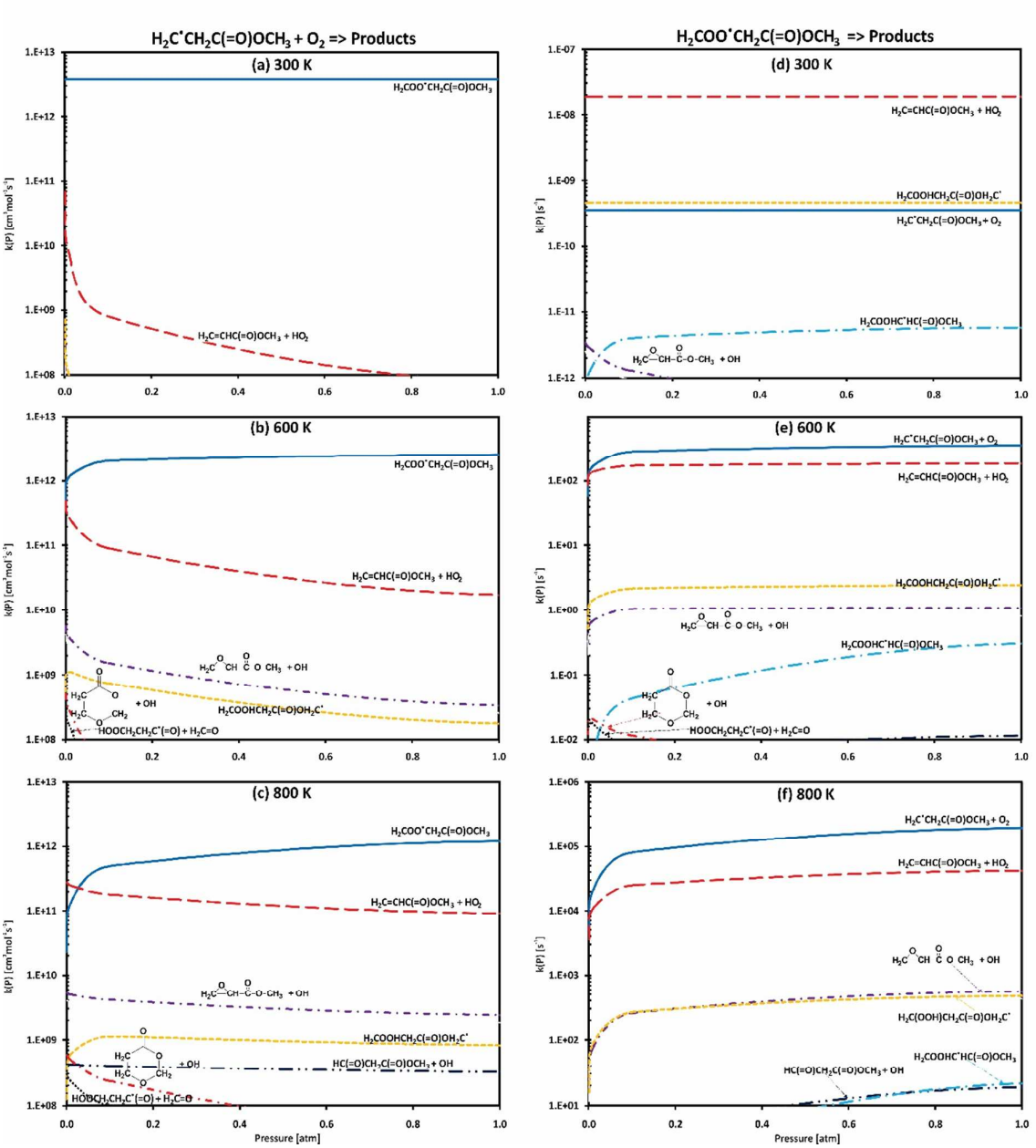

Figure 6. Rate coefficients for $\bullet CH_2CH_2C(=O)OCH_3 + O_2 \rightarrow$ products (**a-c**) and $\bullet OOCH_2CH_2C(=O)OCH_3 \rightarrow$ products (**d-f**) as a function of pressure at 300, 600 and 800 K. Only the most important reaction pathways are shown.

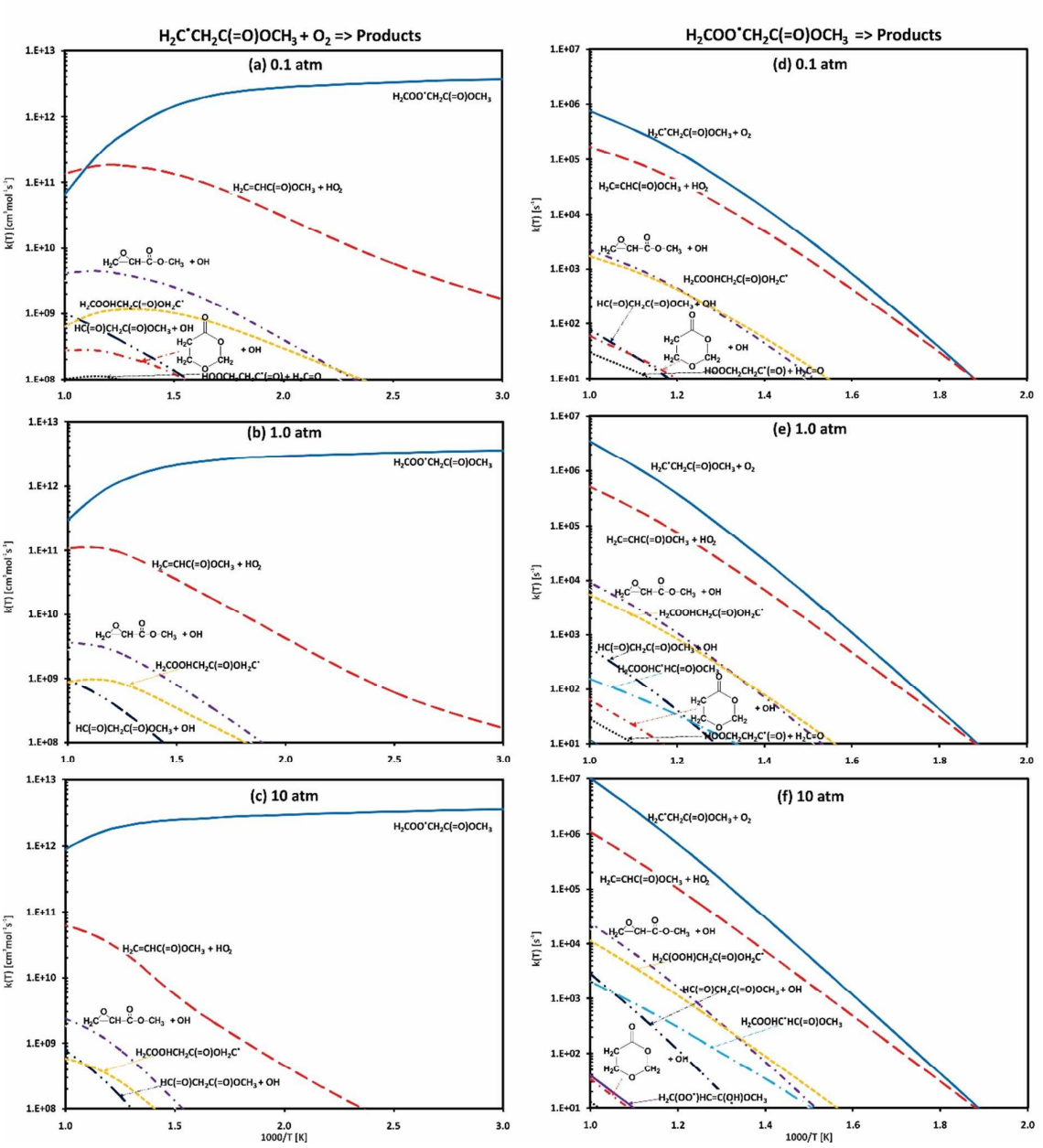

Figure 7. Rate coefficients for $\bullet CH_2CH_2C(=O)OCH_3 + O_2 \rightarrow$ products (**a-c**) and $\bullet OOCH_2CH_2C(=O)OCH_3 \rightarrow$ products (**d-f**) as a function of temperature at 0.1, 1.0 and 10.0 atm. Only the most important reaction pathways are shown.

In this section, we investigate the effect of pressure on rate constants, thus affecting the product distribution. The calculated high-pressure kinetic data are used to compute the pressure- and temperature- dependent rate constants. The QRRK/MSC analysis includes all reaction pathways described in Figures 2-4, except those whose barriers are higher than 12

kcal/mol above the entrance. A complete list of the calculated rate constants in the temperature range 300-1500 K at different pressures (i.e., 0.1, 1.0, and 10 atm) is included in the Supplementary Table S6.

Some representative results, reflecting the effect of pressure at different temperatures (e.g., 300, 600 and 800 K) for both chemically- and thermally- activated reactions for $\bullet CH_2CH_2C(=O)OCH_3 + O_2$ system are presented in Figure 6. Note that because there is almost no change or linear change of k(P) at the pressure higher than 1 atm, the pressure-dependent plots are presented for the presure below 1 atm. The rate constants at different pressures (e.g., 0.1, 1 and 10 atm) for all channels for this system are also presented in Figures 7. Similar plots for $CH_3HC\bullet C(=O)OCH_3 + O_2$ and $CH_3CH_2C(=O)OC\bullet H_2 + O_2$ systems can be found in the supplementary material (Figures S9-S11).

The different pressure dependencies are observed consistently with the earlier discussion as well as the analogous networks for MA + O_2.[39] For three methyl propanoate radicals, the most dominant channel is the formation of the stabilized methyl propanoate peroxy adduct. However, its role decreases with temperature – the higher the temperature, the more important the competing channels are. The stabilization pathways approache the high-pressure limit values near 1.0 atm, while rate constants for chemically-activated bimolecular product channels continue to decrease with increasing pressure (cf. Figures 6). For example, for $\bullet CH_2CH_2C(=O)OCH_3 + O_2$ system, the rate constants decrease from 300 to 800 K ($3.75x10^{+12}$ and $1.20x10^{+12}$ at 1.0 atm, respectively, cf. Figures 6a&c), while rate constants of the other channels increase ($7.09x10^{+7}$ and $9.09x10^{+10}$ at 300 and 800 K, respectively, for $CH_2=CHC(=O)OCH_3 + HO_2$ formation). The ratios of the two most dominant reactions (i.e., **R1**→ **I1** and **R1**→**P3**) at 1.0 atm are $52.9x10^{+3}$ and 13.2 at 300 and 800 K, respectively. The same observation is also true for the other systems; therefore, for the chemically-activated channels, the formation of the adducts (**I1** from **R1**, **I8** from **R2** and **I11**, **I12** from **R3** system)

are dominant, e.g., accounting for more than 99% of the total reactant consumption in the temperature of 300-1500 K and pressure of larger than 1.0 atm. In comparison with the MA + O_2 systems,[39] the difference is noticeable only for the concerted HO_2 elimination of in MP + O_2 systems, which is due to the lack of one C-atom in MA's backbone.

The next section will present the detailed discussion on the first system ($•CH_2CH_2C(=O)OCH_3 + O_2$). The other two systems will be briefly mentioned to highlight the conclusion on the important channels.

$•CH_2CH_2C(=O)OCH_3 + O_2$ system.

As mentioned above, the rate constants of the stabilization channels approximate to the high-rate constant limit at higher pressure as temperature increases (e.g., 0.1 atm and 1 atm at 300 and 600 K, respectively, cf. Figure 6a & 6b), while other rate constants for chemically activated bimolecular product channels continue to decrease with increasing pressure. Due to this reason, it is expected that the complexities involved in chemically activated reaction play a significant role at a low pressure and high temperature region. For example, at 600 and 800 K, the ratios of **R1** → CH_2=CHC(=O)OCH_3 + HO_2 to **R1** → cy[CH_2OCH_2]C(=O)OCH_3 + OH pathways are 52 and 39 at 1.0 atm (cf. Figures 6b & 6c). The rate constant of the concerted elimination of HO_2 channel is higher than that of the cyclization reaction even though the barrier for the latter is much lower with the same size-membered TS ring (27.1 kcal/mol and 18.3 kcal/mol for forming CH_2=CHC(=O)OCH_3 + HO_2 and **R1** → cy[CH_2OCH_2]C(=O)OCH_3 + OH, respectively, cf. Figure 2). It is worth to note, that the cyclization pathway becomes more competitive as temperature increases and pressure decreases because of the arrangement of the transition state via various size-membered ring with a rather high barrier height of 18.3 kcal/mol and 21.0 kcal/mol via 3-membered and 6-membered ring, respectively. Since, as mentioned previously, this process is believed to play

an important role at higher temperature and lower pressure, it is expected to be a sensitive channel to the temperature and pressure.

The picture seems to be even more complicated for the thermally-activated pathways of the initially-formed adduct, where the concerted HO_2 elimination at 300 K (cf. Figure 6d) is the fastest channel. At higher temperature, the most dominant channel is the dissociation back to the reactants **R1,** which is believed to be the main cause for NTC (Negative Temperature Coefficient) behavior for hydrocarbon fuels.[43] Because the concerted elimination channel has the lowest barrier (27.1 kcal/mol compared to 34.0 kcal/mol of the second lowest reaction, re-dissociation to reactants), it only plays a role at lower temperature ($T < 300$ K at $P \approx 1$ atm). As temperature and pressure increase, it becomes more uncompetitive than redissociation, which is because the dissociation back to form reactants **R1** is favored at higher temperature and pressure as mentioned above. Again, the formation of cyclic channel is more competitive as temperature increases; however, it does not compete with the isomerization reaction to form **I2** and **I3** up to 800 K at low pressure of 0.3 atm (cf. Figure 6f). It is noticed that all of the major pathways are near their high-pressure rate constant limit at about 1.0 atm at 600 K (cf. Figure 6e). At higher temperatures, the pre-exponential term of the rate constant becomes increasingly more important, which can be seen in Figure 7. As pressure increases, the stabilization channel approaches the high-pressure limit at about 400–450 K at 1 & 10 atm, cf. Figures 6b & 6c). The stabilization channel still plays the most important role as we expected earlier, especially with increasing pressure, which is similar to the trends for n-$C_3H_7 + O_2$[29] and MA radicals + O_2 systems.[39] In general, the rate constants of other pathways decrease when pressure increases. Note that, as discussed before, the cyclization channel through the various size-membered TS is more affected by pressure. As a result, its rate constant decreases faster with increasing pressure compared to the competitive channels. These complexities illustrate the necessity of proper

accounting for pressure effects. Figures 7d-7f present the pressure effects for the thermally activated channels **I1** → products where the most dominant channel is the redissociation to the reactants, which becomes much more important with increasing pressure at lower temperature. Other pathways (e.g., isomerization, concerted elimination, cyclization, OH-migration and β-scission reactions) are again less competitive in this system.

In conclusion for the $\bullet CH_2CH_2C(=O)OCH_3 + O_2$ system, the important channels (e.g., accounting for more than 99% of the total reactant consumption in the temperature of 300-1500 K and pressure of larger than 1.0 atm) are: (i) formation of the initial adduct from the reactants, **R1→ I1** (Rxn 1 in Table 4); re-dissociation of the adduct back to the reactants, **I1→R1** (Rxn 9) and two reactions of the concerted elimination of HO_2 to form CH_2=CHC(=O)$OCH_3 + HO_2$ (Rxns 2 & 10). Other channels, with much higher barrier as well as undergoing via multiple pathways, do not play a role under low pressure and high temperature conditions. Therefore, at engine-liked conditions (e.g., pressure > 30 atm and 300 K < T < 1000 K) the significance of the four mentioned reactions is expected to be more profound.

Table 4: Simplified MP Radicals + O_2 Submechanism[a] at low-temperature combustion conditions

Radicals + O_2 channel	
$\bullet CH_2CH_2C(=O)OCH_3 + O_2 \rightarrow \bullet OOCH_2CH_2C(=O)OCH_3$	(Rxn. 1)
$\bullet CH_2CH_2C(=O)OCH_3 + O_2 \rightarrow H_2C=CHC(=O)OCH_3 + HO_2$	(Rxn. 2)
$CH_3HC\bullet C(=O)OCH_3 + O_2 \rightarrow CH_3CH(OO\bullet)C(=O)OCH_3$	(Rxn. 3)
$CH_3HC\bullet C(=O)OCH_3 + O_2 \rightarrow H_2C=CHC(=O)OCH_3 + HO_2$	(Rxn. 4)
$CH_3CH_2C(=O)OC\bullet H_2 + O_2 \rightarrow CH_3CH_2C(=O)OCH_2OO\bullet$	(Rxn. 5)
$CH_3CH_2C(=O)OC\bullet H_2 + O_2 \rightarrow CH_3cy[HCC(=O)OCH_2O]$	(Rxn. 6)
$CH_3CH_2C(=O)OC\bullet H_2 + O_2 \rightarrow CH_3HC\bullet C(=O)OCH_2OOH$	(Rxn. 7)
$CH_3CH_2C(=O)OC\bullet H_2 + O_2 \rightarrow CH_3CH_2C(=O)OCHO + OH$	(Rxn. 8)
ROO "delayed" channels	
$\bullet OOCH_2CH_2C(=O)OCH_3 \rightarrow \bullet CH_2CH_2C(=O)OCH_3 + O_2$	(Rxn. 9)
$\bullet OOCH_2CH_2C(=O)OCH_3 \rightarrow H_2C=CHC(=O)OCH_3 + HO_2$	(Rxn. 10)
$CH_3CH(OO\bullet)C(=O)OCH_3 \rightarrow CH_3HC\bullet C(=^{5,6}O)OCH_3 + O_2$	(Rxn. 11)
$CH_3CH_2C(=O)OCH_2OO\bullet \rightarrow CH_3CH_2C(=O)OC\bullet H_2 + O_2$	(Rxn. 12)
$CH_3CH_2C(=O)OCH_2OO\bullet \rightarrow CH_3HC\bullet C(=O)OCH_2OOH$	(Rxn. 13)

$CH_3CH_2C(=O)OCH_2OO\bullet \rightarrow CH_3cy[HCC(=O)OCH_2O]$	(Rxn. 14)
$CH_3CH_2C(=O)OCH_2OO\bullet \rightarrow \bullet CH_2CH_2C(=O)OCH_2OOH$	(Rxn. 15)
$CH_3CH_2C(=O)OCH_2OO\bullet \rightarrow CH_3CH_2C(=O)OCHO + OH$	(Rxn. 16)

[a] Valid in the temperature range of 300-1000 K and P > 1 atm.

$CH_3C\bullet HC(=O)OCH_3$ + O_2 system. The effects of pressure and temperature on the rate constants for this system are shown in Supplementary Figures S2 and S3. It is found that the pressure and temperature dependent trends are similar to the those observed in the $\bullet CH_2CH_2C(=O)OCH_3$ + O_2 system. Specifically, only two chemically-activated channels, namely **R2→I8** and **R2→P**, (Rxns 3 & 4 in Table 4) and one thermally-activated reaction, **I8→R2**) (Rxn 11) are of importance under the conditions of interest. Other pathways (e.g., isomerization and cyclization reactions), are found to be less competitive in this system, at least at the low temperature and high-pressure region, which is due to their higher barrier and multiple pathways.

$CH_3CH_2C(=O)OC\bullet H_2$ + O_2 system. The pressure and temperature dependencies observed in this system are basically consistent with the earlier discussion (cf. Supplementary Figures S4 and S5). Among the three systesms, this system is most complex one; thus the dependencies are expected to be more complicated compared to the other two systems. Due to the position of radical site of the adduct **I11**, $CH_3CH_2C(=O)OC\bullet H_2$ (the radical site at the C-atom bonded to the ester O atom), the concerted HO_2 elimination channel, which plays a role in **R1** and **R2** systems, is missing here. In addition to the missing channel, the availability of low barrier isomerization pathways in this system makes them important in the reaction network. As expected, other pathways such as *β*-scission, OH-migration reactions still play less important role, at least at low pressure and high temperature, which is due to their high barrier heights and multiple-pathway reactions. Similarly, Rxns 12-16 are the most important processes in the $CH_3CH_2C(=O)OCH_2OO\bullet$ → products network. In conclusion, in

spite of the complexities of the full potential energy surface, only four chemically-activated channels (Rxns 5-8 in Table 4) and five thermally-activated reactions (Rxns 12-16) are likely to be important for this system at pressure larger than 30 atm and temperature in the range of 300 -1000 K, while other channels do not play a role at the conditions above due to either higher barriers or happening on a later scale time.

Important Channels

According to the detailed kinetic analysis at common low-temperature combustion conditions in engine (e.g., 300 K < T < 1000 K and P >> 1 atm), Rxns 1-16 (c.f. Table 4) accounts for more than 99% of the overall rate constant for the three MP radicals + O_2 systems while the other channels, such as β-scission and OH-migration, are negliglible. Therefore, despite the complexity of the full potential energy surface, only eight chemically-activated (Rxns. 1-8) and eight thermally-activated (Rxns. 9-16) reactions are of importance under the practical low-temperature combustion conditions.

Comparison with analogous alkyl+O_2 systems

It has been shown previously that the ester group has certain effects on the system reactivity, depending on different reaction types and sites. In order to qualitatively evaluate such effects, we compared our calculated results with previously reported data for analogous alkyl radical + O_2 systems[5, 6] (cf. Figure 8). Specifically, two main reaction types at both primary and secondary sites are considered: (*i*) concerted HO_2 elimination and (*ii*) 1,4 intermolecular H migration from hydroperoxy group (-OOH) to carbon radical site. It is noted that the re-dissociation from the initially-formed adducts between the ester and the non-ester systems (which depends on the ROO• well depth) was discussed in the "Formation of initially-formed adducts" section.

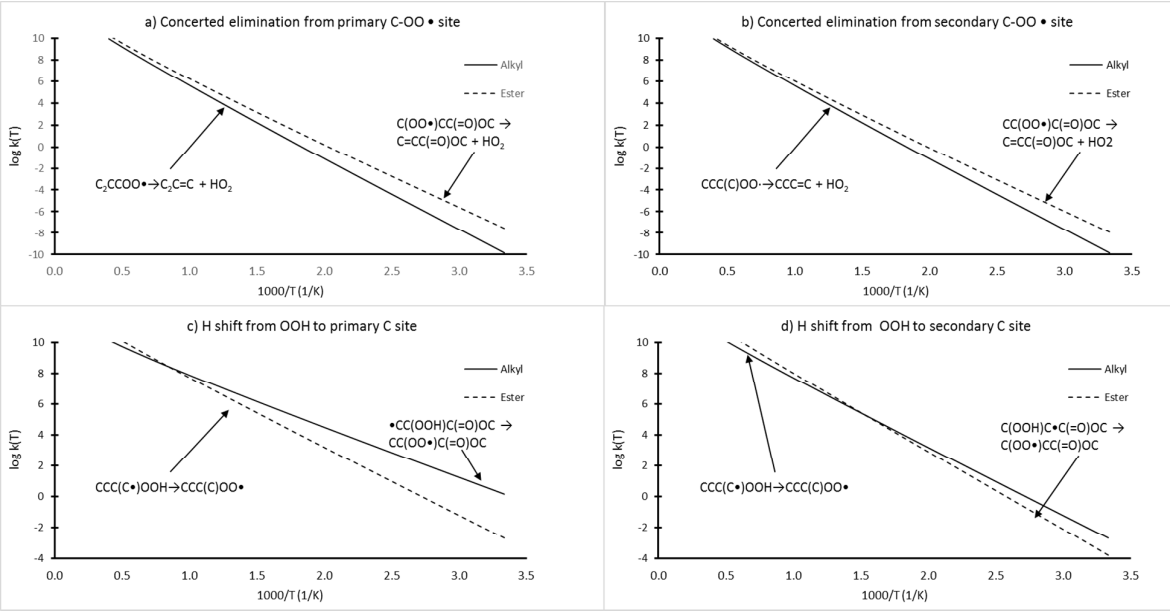

Figure 8: Comparison of high-pressure rate constants for selected reactions between MP radical + O_2 systems (dashed lines, cf. Table 2) and alkyl radical + O_2 systems[5, 6] (solid lines): concerted HO_2 elimination (**a-b**) and 1,4 intermolecular hydrogen migration (**c-d**).

It can be seen that the ester group promotes the concerted H_2O elimination from both primary and secondary COO• site (cf. Figures 8a-b). At low temperature, the rate constants for the ester systems are about 100 times faster and the difference is smaller at higher temperature (e.g., the rate constants are almost the same at T > 2000 K) where the energetic effect is less important. The nature/order of the hydroperoxy site seems to be not of importance to the concerted elimination. For the hydrogen migration reactions (cf. Fig. 8c-8d), it can be seen that the difference between the two systems is more profound at the primary carbon sites, especially in the low temperature region. It is interesting to observe that for this channel the ester group consistently lowers the reaction rate. To shed more light on the difference in A-factors between various cyclic transition states, we plots the pre-exponential factors as a function of temperature for several types of intermolecular hydrogen migrations from C atom to COO· group (cf. Figure 9). For every additional rotor that is tied up in the cyclic transition state, the pre-exponential factor decreases by about an order of magnitude. Similar effects were also observed for the alkyl systems.[5] However, the alkyl

systems (except 1,3 H migration) exhibits almost no temperature dependence which is contrary to the MP + O_2, where A-factors are 10 times larger at T ~2000 K than at 300 K. This difference is attributed to the stronger electrostatic interactions, reflected in the transition state by the subsequent O-O bond fission as its O-O bond is already substantially elongated. This leads to different temperature dependent values for the reaction entropy and, thus, a different temperature dependence as compared to alkyl systems. As pointed out by Davis and Francisco,[61] incorporation of oxygen atoms into the transition state ring significantly changes the energetics. Similarly, it is believed that additional oxygen atoms affects the energetics even stronger, thus even more affecting the temperature dependence of the rate constants.

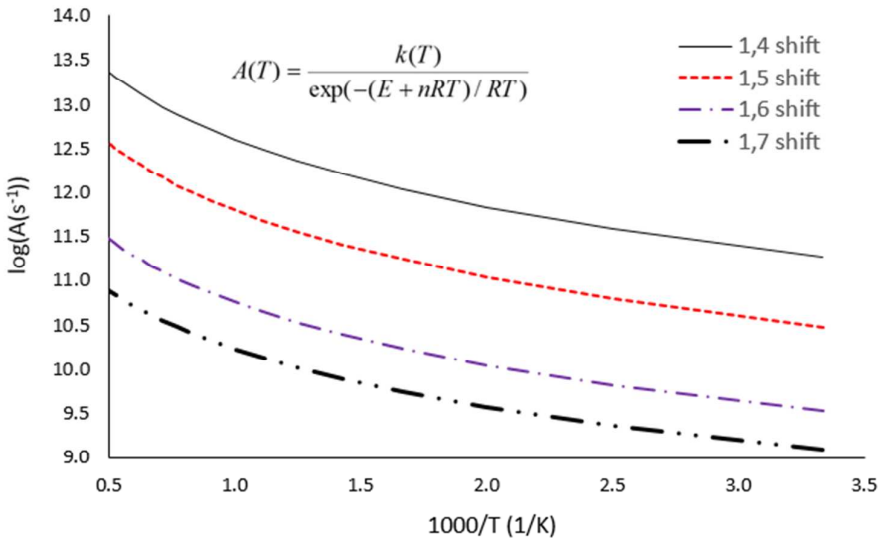

Figure 9: Pre-exponential factors as a function of temperature for the various RO_2 intermolecular H migrations in the titled system from C atom to the COO· group. These values are calculated from the modified Arrhenius fits using *A=k(T)/exp(-(E+nRT)/RT)*), with "*n*" and "*E*" being the parameters in the corresponding modified Arrhenius equation.

The differences in the rate constants for the concerted HO_2 eliminations and hydrogen migrations suggest that rate constants for alkyl systems cannot be assigned for biodiesel systems; thus detailed kinetic studies are needed for such systems to derive reliable high-

pressure rate rules which can be confidently used for real and large biodiesel molecules. Such an effort have been carrying out and will be addressed in separate publications.

4. Conclusions

We have constructed accurate potential energy surfaces for methyl propanoate radicals + O_2 reactions at the CBS-QB3 level of theory. Thermodynamic properties of all species were calculated with explicit corrections for hindered internal rotations. Pressure- and temperature-dependent rates constants for the various possible channels were also derived under the QRRK/MSC framework with high-pressure rate constants obtained from the transition state theory (TST) with explicit Eckart tunneling treatment. We demonstrated that although the detailed PESs lead to a large set of possible reaction pathways, only a few of those play a role in the evolution of the system. It was found, that the presence of the ester group significantly affects the rates of particular complex reaction channels when compared to the similar alkyl + O_2 systems. A thermodynamically consistent detailed kinetic mechanism, consisting of all elementary reactions together with their thermodynamic and kinetic data (given in the accompanied Supplementary Table S6), was constructed for low-temperature oxidation and auto-ignition of the title fuel. The simplified mechanism was also composed specifically for the engine-liked conditions. The mechanism, either full or simplified, can be used as a solid building block to construct detailed kinetic mechanisms for low-temperature combustion of real fuel molecules. This study clearly indicates that methyl propanoate could be a good starting candidate to study biodiesel surrogates with the focus on the role/chemistry of the ester group.

ASSOCIATED CONTENT

Supporting Information Available: (1) Conventional names, short notations and 2-D structures for all species; (2) Tabulated values for reaction barrier and reaction energy at the CBS-QB3 level comparing with other methods for several important channels; (3) Tabulated calculated thermodynamic properties of species are formed from reactions in system; (4) Tabulated calculated thermodynamic properties of radicals are formed from reactions in system; (5) Tabulated values for the high-pressure rate constants of the reactions which have barrier energy larger 10kcal/; (6) Tabulated values for the pressure-dependent apparent rate constants for the various reactions as a function of temperatures at 0.1, 1.0 and 10.0 atm; (7) Tabulated values for electronic structure calculations (geometries, energies, frequencies) for the MP radicals + O_2; (8) Potential energy surfaces for the internal rotations for stable species. (9) Detailed kinetic submechanism (consisting of chem.inp and therm.dat) in CHEMKIN format for MP radicals + O_2 → Products. This material is available free of charge via the Internet.

AUTHOR IMFORMATION

Corresponding Author

*Email: hklam@hcmiu.edu.vn and hklam@icst.org.vn

ACKNOWLEDGMENT

We thank Dr. Carstensen (Ghent University) for helpful discussion and Dr. Villano (Colorado School of Mines) for providing calculation information on alkyl + O_2 systems. Computing resources and financial support provided by the Institute for Computational Science and Technology – Ho Chi Minh City is gratefully acknowledged. This research is also funded by Vietnam National Foundation for Science and Technology Development (NAFOSTED) under grant number 104.03-2012.75. The authors would also like to thank the

computational center of the University of Warsaw (ICM) for providing access to the supercomputer resources and the GAUSSIAN 09 program (Grant G33-03).

REFERENCES

1. Demirbas, A. Biodiesel Production from Vegetable Oils via Catalytic and Non-Catalytic Supercritical Methanol Transesterification Methods. *Prog. Energy Combust. Sci.* **2005,** *31* (5-6), 466-487.
2. Mueller, C. J.; Boehman, A. L.; Martin, G. C. An Experimental Investigation of the Origin of Increased NOx Emissions When Fueling a Heavy-Duty Compression-Ignition Engine with Soy Biodiesel **2009,** *SAE Paper 2009-01-1792*.
3. Rajan, K.; Kumar, K. R. S. Effect of Exhaust Gas Recirculation (EGR) on the Performance and Emission Characteristics of Diesel Engine with Sunflower Oil Methyl Ester *Jordan J. Mech. Ind. Eng.* **2009,** *3*, 306 - 311.
4. Ng, J.-H.; Ng, H. K.; Gan, S. Engine-Out Characterisation using Speed–Load Mapping and Reduced Test Cycle for a Light-Duty Diesel Engine Fuelled with Biodiesel Blends. *Fuel* **2011,** *90* (8), 2700-2709.
5. Villano, S. M.; Huynh, L. K.; Carstensen, H.-H.; Dean, A. M. High-Pressure Rate Rules for Alkyl + O_2 Reactions: Part 1 - The Dissociation, Concerted Elimination, and Isomerization Channels of the Alkyl Peroxy Radical. *J. Phys. Chem. A* **2011,** *115* (46), 13425-13442.
6. Villano, S. M.; Huynh, L. K.; Carstensen, H. H.; Dean, A. M. High-pressure Rate Rules for Alkyl + O_2 Reactions. 2. The Isomerization, Cyclic Ether Formation, and Beta-Scission Reactions of Hydroperoxy Alkyl Radicals. *J. Phys. Chem. A* **2012,** *116* (21), 5068-89.
7. Wang, K.; Villano, S. M.; Dean, A. M. Reactivity-Structure-Based Rate Estimation Rules for Alkyl Radical H Atom Shift and Alkenyl Radical Cycloaddition Reactions. *J. Phys. Chem. A* **2015**, 10.1021/jp511017z.
8. Kim, Y.; Choi, S.; Kim, W. Y. Efficient Basin-Hopping Sampling of Reaction Intermediates through Molecular Fragmentation and Graph Theory. *J. Chem. Theor. Comp.* **2014,** *10* (6), 2419-2426.
9. Vandewiele, N. M.; Van Geem, K. M.; Reyniers, M.-F.; Marin, G. B. Genesys: Kinetic Model Construction Using Chemo-Informatics. *Chem. Eng. J.* **2012,** (207-208), 526-538.
10. Peters, N. D.; Akih-Kumgeh, B.; Bergthorson, J. M. Comparative Analysis of Chemical Kinetic Models Using the Alternate Species Elimination Approach. *J. Eng. Gas Turb. Power.* **2014,** *137* (2), 021505-021505.
11. Van de Vijver, R.; Vandewiele, N. M.; Bhoorasingh, P. L.; Slakman, B. L.; Seyedzadeh Khanshan, F.; Carstensen, H.-H.; Reyniers, M.-F.; Marin, G. B.; West, R. H.; Van Geem, K. M. Automatic Mechanism and Kinetic Model Generation for Gas- and Solution-Phase Processes: A Perspective on Best Practices, Recent Advances, and Future Challenges. *Int. J. Chem. Kinet.* **2015,** *47* (4), 199-231.
12. Green, W. H.; Allen, J. W.; Buesser, B. A.; Ashcraft, R. W.; Beran, G. J.; Class, C. A.; Gao, C.; Goldsmith, C. F.; Harper, M. R.; Jalan, A., et al. *RMG - Reaction Mechanism Generator v4.0.1*, 2013.
13. Guo, J.; Wang, J.; Hua, X.; Li, Z.; Tan, N.; Li, X. Mechanism Construction and Simulation for High-Temperature Combustion of N-Propylcyclohexane. *Chem. Res. Chin. Univ.* **2014,** *30* (3), 480-488.
14. Mersin, I. E.; Blurock, E. S.; Soyhan, H. S.; Konnov, A. A. Hexadecane Mechanisms: Comparison of Hand-Generated and Automatically Generated with Pathways. *Fuel* **2014,** *115*, 132-144.
15. Huynh, L. K.; Lin, K. C.; Violi, A. Kinetic modeling of methyl butanoate in shock tube. *The Journal of Physical Chemistry A* **2008,** *112* (51), 13470-80.

16. Herbinet, O.; Pitz, W. J.; Westbrook, C. K. Detailed Chemical Kinetic Oxidation Mechanism for a Biodiesel Surrogate. *Combust. Flame* **2008,** *154* (3), 507-528.
17. Dooley, S.; Curran, H. J.; Simmie, J. M. Autoignition Measurements and a Validated Kinetic Model for the Biodiesel Surrogate, Methyl Butanoate. *Combust. Flame* **2008,** *153*, 2-32.
18. Huynh, L. K.; Violi, A. Thermal Decomposition of Methyl Butanoate: *ab initio* Study of a Biodiesel Fuel Surrogate. *J. Org. Chem.* **2008,** *73* (1), 94-101.
19. Hayes, C. J.; Burgess, D. R. Exploring the Oxidative Decompositions of Methyl Esters: Methyl Butanoate and Methyl Pentanoate as Model Compounds for Biodiesel. *Proc. Combust. Inst.* **2009,** *32* (1), 263-270.
20. Herbinet, O.; Pitz, W. J.; Westbrook, C. K. Detailed Chemical Kinetic Mechanism for the Oxidation of Biodiesel Fuels Blend Surrogate. *Combust. Flame* **2010,** *157* (5), 893-908.
21. Ismail, H.; Ng, H. K.; Gan, S.; Lucchini, T.; Onorati, A. Development of a Reduced Biodiesel Combustion Kinetics Mechanism for CFD Modelling of a Light-Duty Diesel Engine. *Fuel* **2013,** *106*, 388-400.
22. Wang, Q.-D.; Wang, X.-J.; Liu, Z.-W.; Kang, G.-J. Theoretical and Kinetic Study of the Hydrogen Atom Abstraction Reactions of Ethyl Esters with Hydrogen Radicals. *Chem. Phys. Lett.* **2014,** *616-617*, 109-114.
23. Billaud, F.; Dominguez, V.; Broutin, P.; Busson, C. Production of Hydrocarbons by Pyrolysis of Methyl Esters from Rapeseed Oil *J. Am. Oil Chem. Soc.* **1995,** *72*, 1149-1154.
24. Diévart, P.; Won, S. H.; Gong, J.; Dooley, S.; Ju, Y. A Comparative Study of the Chemical Kinetic Characteristics of Small Methyl Esters in Diffusion Flame Extinction. *Proc. Combust. Inst.* **2013,** *34* (1), 821-829.
25. Chang, A. Y.; Bozzelli, J. W.; Dean, A. M. Kinetic Analysis of Complex Chemical Activation and Unimolecular Dissociation Reactions using QRRK Theory and the Modified Strong Collision Approximation. *Zeitschrift für Physikalische Chemie* **2000,** *214* (11/2000).
26. Frisch, M. J.; Trucks, G. W.; Schlegel, H. B.; Scuseria, G. E.; Robb, M. A.; Cheeseman, J. R.; Scalmani, G.; Barone, V.; Mennucci, B.; Petersson, G. A., et al. *Gaussian 09, Revision A.1*, Gaussian, Inc.: Wallingford CT, 2009.
27. Montgomery-Jr., J. A.; Frisch, M. J.; Ochterski, J. W.; Petersson, G. A. A Complete Basis Set Model Chemistry. VI. Use of Density Functional Geometries and Frequencies. *J. Chem. Phys.* **1999,** *110* (6), 2822-2827.
28. Carstensen, H.-H.; Naik, C. V.; Dean, A. M. Detailed Modeling of the Reaction of $C_2H_5 + O_2$. *J. Phys. Chem. A* **2005,** *109*, 2264-2281.
29. Huynh, L. K.; Carstensen, H. H.; Dean, A. M. Detailed Modeling of Low-Temperature Propane Oxidation: 1. The Role of the Propyl + O_2 Reaction. *J. Phys. Chem. A* **2010,** *114* (24), 6594-607.
30. Tao, H.; Lin, K. C. Pathways, Kinetics and Thermochemistry of Methyl-Ester Peroxy Radical Decomposition in the Low-Temperature Oxidation of Methyl Butanoate: A Computational Study of a Biodiesel Fuel Surrogate. *Combust. Flame* **2014**.
31. Paraskevas, P. D.; Sabbe, M. K.; Reyniers, M.-F.; Papayannakos, N. G.; Marin, G. B. Kinetic Modeling of α-Hydrogen Abstractions from Unsaturated and Saturated Oxygenate Compounds by Hydrogen Atoms. *J. Phys. Chem. A* **2014,** *118* (40), 9296-9309.
32. Paraskevas, P. D.; Sabbe, M. K.; Reyniers, M.-F.; Papayannakos, N.; Marin, G. B. Kinetic Modeling of α-Hydrogen Abstractions from Unsaturated and Saturated Oxygenate Compounds by Carbon-Centered Radicals. *Chem. Phys. Chem.* **2014,** *15* (9), 1849-1866.
33. Paraskevas, P. D.; Sabbe, M. K.; Reyniers, M.-F.; Papayannakos, N.; Marin, G. B. Group Additive Values for the Gas-Phase Standard Enthalpy of Formation, Entropy and Heat Capacity of Oxygenates. *Chem. Eur. J.* **2013,** *19* (48), 16431-16452.

34. El-Nahas, A. M.; Navarro, M. V.; Simmie, J. M.; Bozzelli, J. W.; Curran, H. J.; Dooley, S.; Metcalfe, W. Enthalpies of Formation, Bond Dissociation Energies and Reaction Paths for the Decomposition of Model Biofuels: Ethyl Propanoate and Methyl Butanoate. *J. Phys. Chem. A* **2007,** *111* (19), 3727-39.
35. Hakka, M. H.; Bennadji, H.; Biet, J.; Yahyaoui, M.; Sirjean, B.; Warth, V.; Coniglio, L.; Herbinet, O.; Glaude, P. A.; Billaud, F., et al. Oxidation of Methyl and Ethyl Butanoates. *Int. J. Chem. Kinet.* **2010,** *42* (4), 226-252.
36. Jørgensen, S.; Andersen, V. F.; Nilsson, E. J. K.; Nielsen, O. J.; Johnson, M. S. Theoretical Study of the Gas Phase Reaction of Methyl Acetate with the Hydroxyl Radical: Structures, Mechanisms, Rates and Temperature Dependencies. *Chem. Phys. Lett.* **2010,** *490* (4-6), 116-122.
37. Gonzalez, C.; Schlegel, H. B. An Improved Algorithm for Reaction Path Following. *J. Chem. Phys.* **1989,** *90* (4), 2154.
38. Gonzalez, C.; Schlegel, H. B. Reaction Path Following in Mass-Weighted Internal Coordinates. *J. Phys. Chem.* **1990,** *94* (14), 5523-5527.
39. Mai, T. V. T.; Le, X. T.; Huynh, L. K. Mechanism and Kinetics of Low-Temperature Oxidation of a Biodiesel Surrogate−Methyl Acetate Radicals with Molecular Oxygen. *Struct. Chem.* **2014**.
40. Eckart, C. The Penetration of a Potential Barrier by Electrons. *Phys. Rev.* **1930,** *35* (11), 1303-1309.
41. Poling, B. E.; Prausnitz, J. M.; Connell, O. J. P. *The Properties of Gases and Liquids*. McGraw-Hill: New York, 2000.
42. Ratkiewicz, A.; Bankiewicz, B.; Truong, T. N. Kinetics of Thermoneutral Intermolecular Hydrogen Migration in Alkyl Radicals. *Phys. Chem. Chem. Phys.* **2010,** *12* (36), 10988-10995.
43. Walker, R. W.; Morley, C. Basic chemistry of combustion. In *Low-Temperature Combustion and Autoignition*, Pilling, M. J., Ed. Elsevier: Amsterdam, 1997; pp 1-124.
44. Villano, S. M.; Huynh, L. K.; Carstensen, H.-H.; Dean, A. M. High-Pressure Rate Rules for Alkyl + O_2 Reactions: Part 2 - The Isomerization, Cyclic Ether Formation, and Beta-Scission Reactions of Hydroperoxy Alkyl Radicals. *J. Phys. Chem. A* **2012,** *116*, 5068−5089.
45. Pratt, D. A.; Porter, N. A. Role of Hyperconjugation in Determining Carbon-Oxygen Bond Dissociation Enthalpies in Alkylperoxyl Radicals. *Org. Lett.* **2003,** *5* (4), 387-390.
46. DeSain, J. D.; Taatjes, C. A.; Miller, J. A.; Klippenstein, S. J.; Hahn, D. K. Infrared Frequency-Modulation Probing of Product Formation in Alkyl + O_2 Reactions. Part IV. Reactions of Propyl and Butyl Radicals with O_2. *Faraday Disc.* **2002,** *119* (1), 101-120.
47. Goldsmith, C. F.; Green, W. H.; Klippenstein, S. J. Role of O_2 + QOOH in Low-Temperature Ignition of Propane. 1. Temperature and Pressure Dependent Rate Coefficients. *J. Phys. Chem. A* **2012,** *116* (13), 3325-46.
48. Shiozaki, T.; Gyorffy, W.; Celani, P.; Werner, H. J. Communication: Extended Multi-State Complete Active Space Second-Order Perturbation Theory: Energy and Nuclear Gradients. *J. Chem. Phys.* **2011,** *135* (8), 081106.
49. Ruscic, B.; Pinzon, R. E.; Laszewski, G. v.; Kodeboyina, D.; Burcat, A.; Leahy, D.; Montoy, D.; Wagner, A. F. Active Thermochemical Tables: Thermochemistry for the 21st Century. *J. Phys.: Conf. Series* **2005,** *16*, 561-570.
50. Ruscic, B.; Pinzon, R. E.; Morton, M. L.; Srinivasan, N. K.; Su, M. C.; Sutherland, J. W.; Michael, J. V. Active Thermochemical Tables: Accurate Enthalpy of Formation of Hydroperoxyl Radical, HO_2. *J. Phys. Chem. A* **2006,** *110* (21), 6592-601.
51. Zádor, J.; Taatjes, C. A.; Fernandes, R. X. Kinetics of Elementary Reactions in Low-Temperature Autoignition Chemistry. *Prog. Energy Combust. Sci.* **2011,** *37* (4), 371-421.

52. Kohse-Hoinghaus, K.; Osswald, P.; Cool, T. A.; Kasper, T.; Hansen, N.; Qi, F.; Westbrook, C. K.; Westmoreland, P. R. Biofuel Combustion Chemistry: From Ethanol to Biodiesel. *Angew. Chem. Int. Ed. Engl.* **2010,** *49* (21), 3572-97.
53. Scheer, A. M.; Welz, O.; Zador, J.; Osborn, D. L.; Taatjes, C. A. Low-Temperature Combustion Chemistry of Novel Biofuels: Resonance-Stabilized QOOH in the Oxidation of Diethyl Ketone. *Phys. Chem. Chem. Phys.* **2014,** *16* (26), 13027-13040.
54. Kaiser, E. W. Temperature and Pressure Dependence of the C_2H_4 Yield from the Reaction $C_2H_5 + O_2$. *J. Phys. Chem. A* **1995,** *99* (2), 707-711.
55. Miyoshi, A. Systematic Computational Study on the Unimolecular Reactions of Alkylperoxy (RO_2), Hydroperoxyalkyl (QOOH), and Hydroperoxyalkylperoxy (O_2QOOH) Radicals. *J. Phys. Chem. A* **2011,** *115* (15), 3301-3325.
56. Petway, S. V.; Ismail, H.; Green, W. H.; Estupiñán, E. G.; Jusinski, L. E.; Taatjes, C. A. Measurements and Automated Mechanism Generation Modeling of OH Production in Photolytically Initiated Oxidation of the Neopentyl Radical. *J. Phys. Chem. A* **2007,** *111* (19), 3891-3900.
57. da Silva, G.; Chen, C. C.; Bozzelli, J. W. Toluene Combustion: Reaction Paths, Thermochemical Properties, and Kinetic Analysis for the Methylphenyl Radical + O_2 Reaction. *J. Phys. Chem. A* **2007,** *111* (35), 8663-76.
58. Snitsiriwat, S.; Bozzelli, J. W. Thermochemistry, Reaction Paths, and Kinetics on the Tert-Isooctane Radical Reaction with O_2. *J. Phys. Chem. A* **2014,** *118* (26), 4631-46.
59. Allen, J. W.; Goldsmith, C. F.; Green, W. H. Automatic Estimation of Pressure-Dependent Rate Coefficients. *Phys. Chem. Chem. Phys.* **2012,** *14* (3), 1131-55.
60. Carstensen, H.-H.; Dean, A. M. The Kinetics of Pressure-Dependent Reactions. *Compr. Chem. Kinet.* **2007,** *42*, 105-187.
61. Davis, A. C.; Francisco, J. S. *Ab initio* Study of Hydrogen Migration across n-Alkyl Radicals. *J. Phys. Chem. A* **2011,** *115* (14), 2966-2977.